Inorganic Chemistry

ARTICLE

pubs.acs.org/IC

Probing the Nature of the Co^{III} Ion in Corrins: The Structural and Electronic Properties of Dicyano- and Aquacyanocobyrinic Acid Heptamethyl Ester and a Stable Yellow Dicyano- and Aquacyanocobyrinic Acid Heptamethyl Ester

Susan M. Chemaly,*[,†] Kenneth L. Brown,[§] Manuel A. Fernandes,[†] Orde Q. Munro,*[,‡] Craig Grimmer,[‡] and Helder M. Marques*[,†]

[†]Molecular Sciences Institute, School of Chemistry, University of the Witwatersrand, PO Wits, Johannesburg, 2050 South Africa

[‡]School of Chemistry, University of KwaZulu-Natal, Scottsville, Pietermaritzburg, 3209 South Africa

[§]Department of Chemistry, Ohio University, Athens, Ohio 45701, United States

Supporting Information

ABSTRACT: A stable yellow derivative of cobyrinic acid heptamethyl ester, (5*R*,6*R*)-Coα,Coβ-dicyano-5,6-dihydro-5-hydroxy-heptamethylcob(III)yrinate-*c*,6-lactone (DCSYCbs), was prepared from dicyanocobyrinic acid heptamethyl ester (DCCbs). The C5 carbon is oxidized and the *c* side chain cyclized to form a lactone at C6; the 13 atom, 14 π-e^- delocalized system of corrins is interrupted, giving a triazamethine system with four conjugated double bonds between N22 and N24 and an isolated double bond between N21 and C4. Stable yellow aquacyanocobyrinic acid heptamethyl ester (ACSYCbs) was prepared by driving off HCN with N_2 in a methanol/acetic acid solution. The electronic spectra of DCCbs and DCSYCbs appear similar except that the bands in DCSYCbs are shifted to shorter wavelengths and the γ-band is much less intense. The experimental spectra were adequately modeled using TD-DFT at the PBE1PBE/6-311G(d,p) level of theory. DCSYCbs crystallizes in the space group $P2_12_12_1$ (R_1 = 6.08%) with Z = 4, including one methanol solvent molecule and one water molecule per cobester. The addition of a hydroxyl group at C5 causes loss of the double bond between C5 and C6 and elongation of the C5−C6 bond. From a combination of two-dimensional ^{1}H TOCSY and ROESY NMR spectra and ^{1}H/^{13}C HSQC and HMBC data, the complete ^{1}H and ^{13}C NMR assignments of DCSYCbs were possible, except for two of the ester methyl groups and the ^{13}C resonances of the two axial cyanide ligands. The latter were assigned using relative chemical shifts calculated by GIAO-DFT methods. The ^{59}Co resonance of DCCbs was observed at 4074 ppm while that of DCSYCbs is shifted downfield to 4298 ppm. Comparison with available ^{59}Co data of analogous systems suggests that the more π-conjugated corrin of DCCbs interacts more strongly with the metal than the less extensively conjugated macrocycle of DCSYCbs. As the strength of the interaction between Co(III) and an equatorial macrocycle increases, ν_{CN} of axially coordinated CN^- shifts to lower frequency; in DCSYCbs and DCCbs ν_{CN} occurs at 2138 and 2123 cm^{-1}, respectively. Hence the corrin ligand in DCCbs interacts more strongly with the metal than the stable yellow corrin ligand, with its diminished conjugation. The UV−vis spectral data and DFT-calculated MOs are consistent with greater overlap between the corrin and the metal orbitals in DCCbs relative to DCSYCbs, which gives the metal in the former a softer, more covalent character.

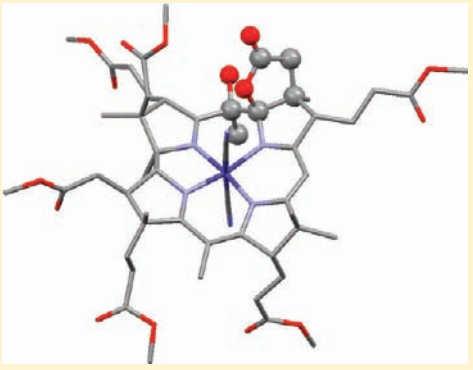

INTRODUCTION

Cr(III) and Co(III) are the classical examples of inert transition metal ions from the first row of the d block. The residence time of water in the inner coordination sphere of the aquated Co(III) ion, as determined by NMR methods, is 10^5 s,[1] and 1.8×10^5 to 2.2×10^5 s for Cr(III).[2] By comparison, the residence time is 8.8×10^{-7} s in $[Co(H_2O)_6]^{2+}$;[3] 6×10^{-3} to 5×10^{-5} s in $[Fe(H_2O)_6]^{3+}$;[4−6] and 3.7×10^{-5} s in $[Ni(H_2O)_6]^{2+}$.[3] Thus, one of the notable features of the chemistry of Co(III) in the cobalt corrins (vitamin B_{12} and its derivatives) is its lability toward ligand substitution (for example, refs 7−21). Data for the reaction symbolized by eq 1, where entering L displaces X *trans* to Y in Co(III) complexes with four N-donor equatorial ligands (N_4), are instructive. When L = SCN^-, X = Y = H_2O, the second-order rate constant, k_2, is 8.6×10^{-7} M^{-1} s^{-1} for $N_4 = (NH_3)_4$,[22] but 9 orders of magnitude larger (8.2×10^2 M^{-1} s^{-1}) when N_4 = corrin.[23] For L = CN^-, X = H_2O, and Y = Me, $k_2 = 2 \times 10^2$ M^{-1} s^{-1} for N_4 = bis(ethylenediamine), but the reaction is too fast to be measured by stopped flow methods when N_4 = corrin.[24]

$$Y - Co^{3+}(N4) - X + L \rightarrow Y - Co^{3+}(N_4) - L + X \quad (1)$$

Received: February 10, 2011
Published: August 18, 2011

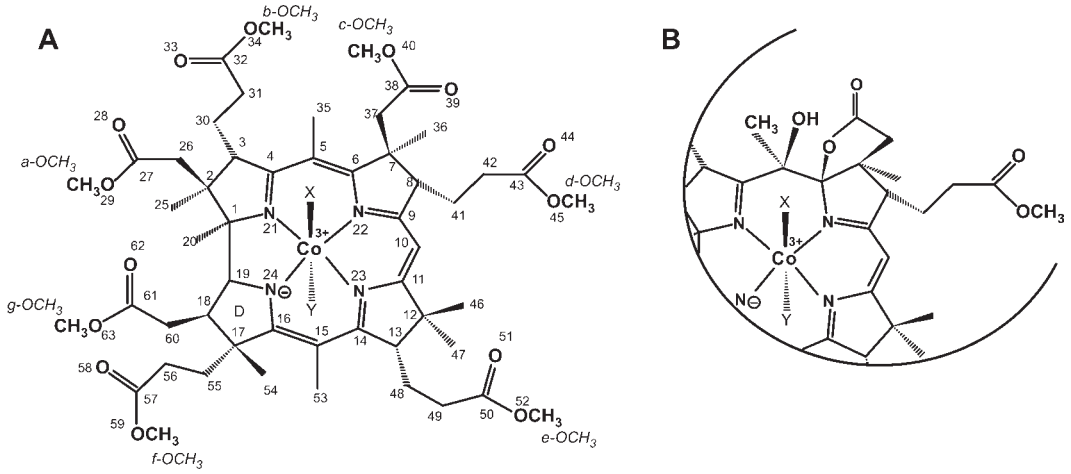

Figure 1. Cobalt corrins referred to in this work and the numbering used. The "upper" ligand X is on the β face of the corrin and the "lower" ligand Y is on the α face. In this standard view of the corrins, the "western" half of the molecule contains the C1−C19 bond and C10 is in the "eastern" half of the molecule. (A) Dicyanocobester (DCCbs, X = Y = CN^-); X = H_2O, Y = CN^- and X = CN^-, Y = H_2O, the two diastereomers of aquacyanocobester (ACCbs). (B) The stable yellow cobester with interrupted conjugation at C5. Dicyano-stable yellow cobester (DCSYCbs) has X = Y = CN^- while aquacyano-stable yellow cobester (ACSYCbs) consists of two diastereomers, X = H_2O, Y = CN^- and X = CN^-, Y = H_2O.

The extent of unsaturation of the equatorial ligand seems to be an important factor in determining the rate of the substitution of an axial ligand. For L = H_2O, X = Y = Cl^-, the rate constants vary in the ratio 1:36:270 as N_4 is varied from cyclam (abbreviation for 1,4,8,11-tetraazacyclotetradecane, [16-ane]-N4), to *trans*[14]diene, to cobaloxime (abbreviation for bis-(dimethylglyoximato)).[25] As we have pointed out before,[19,26] the approximate lability ratio of the metal ion toward substitution in corrin, porphyrin, cobaloxime, and tetra-ammine systems is 10^9:10^6:10^4:1.

The kinetic evidence suggests that labilization of the axial ligand increases with the extent of delocalization of the *cis* π electron system (ammine ≈ cyclam < *trans*[14]diene < cobaloxime < porphyrin) and inversely with the size of the macrocyclic cavity (porphyrin < corrin). We have suggested that this kinetic *cis* effect is the consequence of the delocalization of electron density between the equatorial ligands and the metal, making the metal softer, and imparting to it a more labile Co(II)-like character.[19,26,27] If this is indeed the case, one might expect lability to increase as (i) the polarizability of the *cis* ligand increases and/or (ii) the macrocyclic cavity size decreases and the orbital overlap between the *cis* donors and the metal increases.

Cis effects are important in corrin chemistry. For example, the electronic spectra of the cobalamins are dominated by $\pi \rightarrow \pi^*$ transitions of the corrin ring[28−31] that are strongly dependent on the axial ligand.[27,30,32] The C10−Cl bond length in X-10-ClCbls (Cbl = cobalamin), in which the C10 H is replaced by Cl, depends strongly on the polarizability of the axial ligand, X.[19] Substitution of the C10 H by an electron-withdrawing group such as NO deactivates the axial coordination site toward ligand substitution.[33] This all suggests that the axial ligand chemistry of a cobalt corrin can be modified by perturbing the electronic structure of the corrin ring.

There is already evidence in this regard. The substitution of C10 H by Cl causes the pK_a of coordinated H_2O to drop from 8.09 to 7.65 at 25 °C, and semiempirical molecular orbital (SEMO) calculations on the hydroxo complexes show that charge density is delocalized from the axial donor atom to the metal and Cl, causing coordinated OH^- to be a poorer base in HO-10-ClCbl than in HOCbl.[26] Because of the greater ability of the metal, in concert with the C10 Cl, to accept charge density from the axial ligand, an anionic ligand will bind more strongly to Co(III) in the 10-chloro derivative than to aquacobalamin (B_{12a}) itself, and log K values are between 0.10 and 0.63 higher; conversely, neutral N-donor ligands bind preferentially to B_{12a} with log K values between 0.17 and 0.30 higher. The replacement of coordinated H_2O in H_2O−10−$ClCbl^+$ by pyridine and azide proceed by an interchange mechanism under dissociative activation;[26] values of $\Delta H^{\ddagger}$ and $\Delta S^{\ddagger}$ are less positive for the reaction of these ligands with H_2O−10−$ClCbl^+$ than with B_{12a}, indicative of an earlier transition state. In the temperature range 5−35 °C, H_2O−10−$ClCbl^+$ reacts more slowly than B_{12a}; SEMO calculations showed that as the Co−O bond to departing H_2O is stretched, the charge on the metal is always larger in B_{12a} than in the 10-chloro derivative, and the former is always the better electrophile toward the entering ligand.

To further examine the connection between the electronic structure of corrin and the behavior of the cobalt corrin toward an equatorial ligand, we have prepared a derivative of the heptamethyl ester of cobyrinic acid, (5*R*,6*R*)-Coα,Coβ-dicyano-5,6-dihydro-5-hydroxy-heptamethylcob(III)yrinate-*c*,6-lactone (which we shall refer to as a "stable yellow cobester", DCSYCbs, Figure 1), from the corresponding dicyanocobyrinic acid heptamethyl ester, Coα,Coβ-dicyano-heptamethylcob(III)yrinate (DCCbs, Figure 1), in which the 13 atom, 14 π-e^- delocalized system of normal corrins is interrupted by oxidation of the C5 carbon, leading to a 10 π-e^- system between N21 and N24, and an isolated double bond between N21 and C4. The compound, originally reported by Gossauer, Grüning, and co-workers,[34,35] was characterized by mass spectrometry, infrared spectroscopy, ^{1}H, ^{13}C, and ^{59}Co NMR spectroscopy, UV−vis and CD spectroscopy, and single crystal X-ray diffraction. From the spectroscopic evidence we deduce that the diminished conjugation of the corrin in DCSYCbs increases the hardness of Co(III) in the corrin. The consequences of this for the thermodynamics and kinetics of ligand substitution reactions are examined in the accompanying paper.[36]

dx.doi.org/10.1021/ic200285k |*Inorg. Chem.* 2011, 50, 8700–8718

EXPERIMENTAL SECTION

Instrumentation. UV−vis spectra were recorded in 1-cm quartz cuvettes on a Cary 1E or Cary 300 UV−vis spectrophotometer. The temperature of the cell block was maintained (±0.1 °C) by a water-circulating bath and measured with a thermistor device. CD spectra were recorded in 1-mm quartz cuvettes on a Jasco J-810 spectropolarimeter at 5 °C. IR spectra were recorded in the solid state using a diamond anvil cell with a Bruker Tensor IR spectrometer. Intensity data were collected on a Bruker APEX II CCD area detector diffractometer with graphite monochromated Mo Kα radiation (50 kV, 30 mA) using the *APEX 2*[37] data collection software. The collection method involved ω-scans of width 0.5° and 512 × 512 bit data frames. Data reduction was carried out using the program *SAINT+*[38] and absorption corrections made using *SADABS*.[39] One-dimensional ^{1}H, two-dimensional proton homonuclear (TOCSY, ROESY), and two-dimensional heteronuclear ($^{1}H-^{13}C$) experiments (HSQC, HMBC) were carried out on a Bruker DRX 800 MHz spectrometer using an inverse detection cryoprobe. One dimensional $^{13}C-\{^{1}H\}$ proton decoupled spectra were obtained on a Bruker DRX 600 MHz spectrometer using a broadband probe. All ^{1}H and ^{13}C NMR data were collected at 25 °C. We also recorded the one-dimensional ^{1}H, ^{13}C, and ^{59}Co NMR spectra at 30 °C K on a Bruker Avance III 500 spectrometer equipped with a 5-mm BBOZ probe operating at 500 MHz (^{1}H), 125 MHz (^{13}C), and 118 MHz (^{59}Co frequency) on 10 mg samples dissolved in 600 μL of $CDCl_3$ (99.8% deuteration, stabilized with silver foil, dried over CaH_2). FAB mass spectra were obtained using a VG 70SE magnetic sector mass spectrometer, Ion Tech Saddlefield, and atom gun at 8 tV with xenon gas; ESI mass spectra were obtained using a Thermo LXQ ion trap mass spectrometer with ESI source. The pH was measured using a Metrohm 720 or 827 pH meter with a Unitrode or Biotrode electrode calibrated at pH 7.00 and 9.00 with standard buffers. TLC was performed on Alugram Sil G/UV_{254} silica gel plates from Machery-Nagel. HPLC was performed using an Ultimate 3000 pump and photodiode array detector with Chromoleon Chromatographic Management System software and a normal phase silica column (Phenomenex Luna Silica 5 μ, 250 mm × 4.60 mm) or a reverse phase C18 column (Phenomenex Luna C18 5 μ, 150 mm × 4.60 mm). Isocratic elution with methanol was used for separations on the silica column, flow rate 1 mL min^{-1} (350 psi); for those on the C18 column either gradient elution, ammonium phosphate buffer pH 3.0, 0.025 M (100%) to methanol (100%) over 15 min, or isocratic elution with methanol was used, flow rate 1 mL min^{-1} (350 psi)

Preparation and Characterization of Coα,Coβ-dicyano-heptamethylcob(III)yrinate (Dicyanocobester, DCCbs, Figure 1A) and Its Aquacyano Form. This was prepared according to the procedure of Werthemann.[40] In a typical preparation, cyanocobalamin (1.3 g), dissolved in a solution of *ca.* 1 M sulfuric acid in methanol (160 mL), was refluxed for four days under N_2. The solution was concentrated (to about 50 mL) by rotary evaporation, diluted with water (about 200 mL), and neutralized with sodium carbonate to produce a red solution. Potassium cyanide (0.71 g) was added (turning the solution purple), and the solution was extracted first with trichloroethylene (3 × 200 mL) and then with dichloromethane (3 × 200 mL). Trichloroethylene was used as a substitute for carbon tetrachloride in the original procedure; it was chosen because it has a similar polarity index (1.0) and solubility in water (0.11%) to carbon tetrachloride (1.6% and 0.08%, respectively).[41] The trichloroethylene extract was rotary evaporated to dryness. The dichloromethane extract, which contained monocarboxylic acid derivatives of DCCbs,[42] was again refluxed and the procedure repeated. The trichloroethylene extracts were combined and purified by column chromatography (38 cm × 2.5 cm) on a mixture of silica gel (75 g) and potassium cyanide (2 g) with 2:3 (v/v) toluene/methyl acetate as eluent[43] in 57% yield. It is important to use a less polar solvent than dichloromethane for the extraction of DCCbs; if only dichloromethane is used, then the monocarboxylic acid impurity is coextracted, and this seriously compromises the efficiency of the subsequent column separation. TLC (silica gel, ethyl acetate/methanol/toluene 9.5:1.0:0.5) of DCCbs shows a single purple spot at R_f 0.62. HPLC (C18 column, chloroform:methanol) shows a sharp peak at R_t 6.6 min (99.9%). CD spectrum (1.23×10^{-4} M DCCbs in 0.01 M KCN in 10:1 v/v water/ethanol, Figure S1), λ/nm (CD/millidegree): 582 (−0.84), 555 (−1.87), 525 (−2.93), 500 (−1.32), 420 (3.40), 416 (3.28), 397 (5.36), 367 (1.33), 348 (−3.04), 327 (−1.91), 310 (−3.07), 278 (0.61), 252 (−2.70), 220 (+3.58). UV−vis, λ/nm, $\varepsilon/10^3$ M^{-1} cm^{-1}: 580 (10.1), 550 (8.67), 369 (30.4), 308 (10.1), 276 (10.4). MS-ESI: 1087.2 $(M - H)^-$. MS-ESI^+: 1062.6 $(M - CN^-)$. IR, ν/cm^{-1}: 2123 (C≡N str), 1726 (C═O str).

Aquacyanocobester (ACCbs) was prepared in quantitative yield by dissolving DCCbs (39 mg) in 25 mL of methanol containing glacial acetic acid (pH 3.0) and passing a slow stream of N_2 through the solution for 24 h,[43,44] monitored by UV−vis spectroscopy as the color changed from purple to red, followed by rotary evaporation to dryness. TLC (silica gel, dichloromethane/methanol 9:1 v/v) of ACCbs shows two red spots at R_f 0.88 and 0.94, due to the two diastereomers (α-H_2O, β-CN and α-CN, β-H_2O). HPLC (C18 column, phosphate buffer pH 3/methanol) shows two peaks at 1.9 min (58%) and 4.4 min (42%). UV−vis, λ/nm, $\varepsilon/10^3$ M^{-1} cm^{-1}: 497 (8.35), 353 (25.4), 272 (11.6). MS-FAB: 1080.4 $(M)^+$, 1062.5 $(M - H_2O)^+$, 1037.5 $(M - CN - H_2O, + H,e)^+$. IR, ν/cm^{-1}: 2129 (C≡N str), 1728 (C═O str).

Preparation and Characterization of (5*R*,6*R*)-Coα,Coβ-dicyano-5,6-dihydro-5-hydroxy-heptamethylcob(III)yrinate-*c*,6-lactone (Dicyano-Stable Yellow Cobester, DCSYCbs, Figure 1B) and Its Aquacyano Form. DCSYCbs was prepared by refluxing a mixture of DCCbs (100 mg), ascorbic acid (400 mg), sodium bicarbonate (210 mg), methanol (15 mL), sodium phosphate buffer pH 7.2 (16 mL, *ca.* 0.5 M), and EDTA (10 mM) at 65 °C for 3 h with a slow stream of O_2 passing through the solution. The color changed from purple to yellow-brown. After cooling to room temperature, saturated sodium chloride solution (20 mL) was added and the solution extracted with small portions of dichloromethane until no more yellow color was extracted into the organic layer; this was filtered through a cotton-wool plug and rotary evaporated to dryness.[34,44] Unreacted DCCbs (purple) and DCSYCbs (orange-yellow) were isolated from the dichloromethane extract by column chromatography (40 cm × 2.5 cm) on silica gel (80 g) containing potassium cyanide (2 g), using 97:3 v/v dichloromethane/methanol as eluent. The DCSYCbs fraction was purified on a second column (15 cm × 1.5 cm) containing silica gel (20 g) and potassium cyanide (1 g), using the same eluent, filtered through a cotton-wool plug and rotary evaporated to dryness; the yield was 10%. UV−vis, λ/nm, $\varepsilon/10^3$ M^{-1} cm^{-1}: 484 (10), 319 (12). MS-FAB: 1089.7 $(M)^+$, 1063.7 $(M - CN)^+$; MS-ESI^+: 1064.5 $(M - CN)^+$. IR, ν/cm^{-1}: 2136 (C≡N str), 1780 (C═O str, lactone), 1727 (C═O str, ester). HPLC (silica column, methanol) shows a single sharp peak at R_t 2.3 min (99.6%).

Aquacyano-stable yellow cobester (ACSYCbs) was prepared in quantitative yield by dissolving DCSYCbs (14 mg) in 25 mL methanol containing glacial acetic acid (pH 3.0) and passing a slow stream of N_2 through the solution for 24 h to remove HCN; the reaction was monitored by UV−vis spectroscopy as the color changed from orange-yellow to yellow-brown. After conversion was complete the solution was rotary evaporated to dryness. UV−vis, λ/nm, $\varepsilon/10^3$ M^{-1} cm^{-1}: 484 (10), 319 (12). MS-FAB: 1064.5 $(M - H_2O)^+$, 1038.5 $(M - CN - H_2O)^+$. IR, $\bar{\nu}/cm^{-1}$: 2137 (C≡N str), 1780 (C═O str, lactone), 1730 (C═O str, ester). HPLC (isocratic elution, C18 column, methanol) shows two poorly resolved peaks at 2.4 min (*c.* 91%) and 2.7 min (*c.* 9%).

Structure Determination of DCSYCbs. Slow evaporation of a methanol solution of DCSYCbs at room temperature produced short rodlike orange crystals. The crystal structure was solved by direct

Table 1. Crystal Data and Structure Refinement for Dicyano-Stable Yellow Cobester (DCSYCbs)

CCDC deposition number	807935
empirical formula	C54 H77 Co N6 O17
fw	1141.15
T/K	173(2)
wavelength /Å	0.710 73
cryst syst	orthorhombic
space group	$P2_12_12_1$
unit cell dimensions /Å	a = 9.4852(4)
	b = 18.9342(8)
	c = 31.3583(13)
V/Å^3	5631.8(4)
Z	4
density (calculated)/Mgm^{-3}	1.346
abs coeff/mm^{-1}	0.380
F(000)	2424
cryst size/mm^3	0.29 × 0.10 × 0.03
θ range for data collection/deg	1.69 to 25.49
index ranges	$-11 \le h \le 11$
	$-22 \le k \le 22$
	$-37 \le l \le 28$
reflns collected	35 872
indep reflns	10 493 [R(int) = 0.1143]
completeness to θ = 25.49°	100.0%
abs corr	none
refinement method	full-matrix least-squares on F^2
data/restraints/params	10 493/80/718
GOF on F^2	0.997
final R indices ($I > 2\sigma(I)$)	R1 = 0.0608, wR2 = 0.1218
R indices (all data)	R1 = 0.1290, wR2 = 0.1474
abs structure param	−0.02(2)
largest diff peak and hole/e Å^{-3}	0.950 and −0.811

methods using SHELXTL.[45] Non-hydrogen atoms were first refined isotropically followed by anisotropic refinement by full matrix least-squares calculations based on F^2 using SHELXTL. All H atoms were positioned geometrically and allowed to ride on their parent atoms. MERCURY[46] and ORTEP-3[47] were used to produce publication materials. The experimental data for the crystal structure determination are given in Table 1.

NMR Spectroscopy. For spectra collected on a Bruker DRX 800 MHz spectrometer, the sample contained 21 mg of DCSYCbs dissolved in 0.8 mL of 100.0 atom % D chloroform-*d* (Aldrich) containing 0.03% v/v TMS. The ^{1}H-two-dimensional TOCSY (States-TPPI phase-sensitive method) data were collected into a 400 × 2048 data matrix with 32 scans per t_1 value. A spectral width of 9600 Hz (12 ppm) was used with a 1.4 s relaxation delay between scans. Two such experiments were performed with 18 and 67 ms mixing delays to permit sequential assignments of spin systems. The ^{1}H-two-dimensional ROESY data were also collected into a 400 × 2048 data matrix but with 64 scans per t_1 value. The spectral width was also 9600 Hz, and the relaxation delay was 1.4 s. The mixing time was 200 ms.

The phase-sensitive HSQC data were collected into a 256 × 2048 data matrix with a 205 ppm spectral width in the ^{13}C (F1) dimension and a 12 ppm spectral width in the ^{1}H (F2) dimension. Scans (32) were taken per t_1 value with a 1.2 s relaxation delay. The HMBC data was collected into a 256 × 2048 ($t_1 \times t_2$) data matrix with 205 and 12 ppm spectral widths in the F1 and F2 frequency dimensions, respectively. Scans (128) were collected per t_1 value with a 2 s relaxation delay between scans.

For data acquired on a Bruker Avance III 500 MHz NMR spectrometer, ^{59}Co NMR spectra were recorded at a transmitter frequency of 119.123774 MHz (spectral frequency, 118.638 457 MHz) using a standard single 90° pulse sequence (9.0 μs 90° pulse at 0.0 dB; recycle time, 1 s) and a spectral width of 2000 ppm comprising 6.4 × 10^4 data points. Spectra were processed using an exponential line-broadening function with a 100 Hz line-broadening factor. Chemical shifts were referenced externally to a saturated solution of $K_3[Co(CN)_6]$ in D_2O at 303 K. ^{13}C spectra for DCCbs and DCSYCbs were recorded at a transmitter frequency of 125.74 MHz using the standard Bruker pulse sequence (single 30° pulse with power-gated composite-pulse decoupling of ^{1}H, modulation mode Waltz-16, sw 261.6 ppm; 64 K data points; 90 pulse 9.9 us at 1.7 dB; recycle time 3.00 s). ^{13}C spectra were processed with 2-fold zero-filling and an exponential line-broadening weighting function with a 1 Hz line-broadening factor. ^{13}C chemical shifts were referenced relative to $CDCl_3$ (77.0 ppm).

Computational Work. *Gaussian 03*[48] was used for all DFT simulations with the hybrid functional PBE1PBE[49] and a 6-311G(d,p) basis set to compare the electronic structures of DCCbs and DCSYCbs. In each case, the starting points for the geometry optimizations were the crystal structures of the relevant cobester. Full frequency calculations were used on the optimized geometries to confirm that the energy-minimized structures were true minima (all optimized geometries gave zero imaginary modes). NMR shielding tensors were calculated on the *in vacuo* energy-minimized structures using the GIAO method.[50] Gas phase shielding tensors were augmented with simulations in methanol and chloroform solvent continua using an IEF-PCM model.[51] Calculated chemical shifts for DCCbs and DCSYCbs are given relative to TMS (^{1}H and ^{13}C) and $[Co(CN)_6]^{3-}$ (^{59}Co) with the reference data calculated at the same level of theory as the cobalt corrinoid derivatives. Electronic spectra were calculated *in vacuo* using the TD-DFT method;[52] 22 singlet excited states were located with energies ranging from 1.55 to 2.48 eV (250−500 nm) for DCCbs and DCSYCbs. By scaling the state energies and molar absorptivities to allow the experimental and calculated γ-bands to coincide and by using a summation of component Gaussian bands with a full-width-at-half-maximum (fwhm) of 775 cm^{-1} for the calculated states, absorption envelopes suitable for comparison with the experimental spectra were obtained.

UV−Vis Spectra. The concentrations of cobesters and stable yellow cobesters in solution were determined by addition of excess KCN to give DCCbs (ε_{368} 3.0 × 10^{-4} L mol^{-1} cm^{-1})[43] and DCSYCbs (ε_{487} 1.0 × 10^{-4} L mol^{-1} cm^{-1}),[34] respectively.

The UV−vis spectra of DCCbs and DCSYCbs were determined in the presence of excess KCN to remove traces of ACCbs and ACSYCbs. The spectra were resolved by Gaussian deconvolution[27] using the Multipeak Fitting function of the program *Igor Pro*.[53] The spectrum was converted to a plot of extinction coefficient vs wavenumber and fitted to eq 2 where ε_T is the total extinction coefficient, $\bar{\nu}$ the measured wavenumber, $\bar{\nu}_j$ the wavenumber at which the jth Gaussian component reaches a maximum extinction coefficient, ε_j the extinction coefficient of the jth peak, and Δ_j the fwhm of the jth peak.

$$\varepsilon_T = \sum_{j=1}^{n} \varepsilon_j \exp\left[\frac{-(\bar{\nu} - \bar{\nu}_j)^2}{2\Delta_j^2}\right] \quad (2)$$

pK_a of ACCbs and ACSYCbs. Coordinated H_2O in both ACCbs and ACSYCbs will dissociate (eq 3, [Cor] = corrin) with a pK_a below that of H_2O because of the polarizing effect of the metal. For aquacyanocobinamide pK_a = 11.0.[54−56]

$$[CN - Co[Cor] - OH_2]^+ \rightleftharpoons [CN - Co[Cor] - OH] + H^+ \quad (3)$$

dx.doi.org/10.1021/ic200285k |*Inorg. Chem.* 2011, 50, 8700–8718

Table 2. UV−Vis Spectra of Cobesters in Sodium Phosphate Buffer (pH 8.00, μ 0.1)

DCCbs		ACCbs		DCSYCbs		ACSYCbs	
λ /nm	ε /10^3 M^{-1} cm^{-1}	λ /nm	ε /10^3 M^{-1} cm^{-1}	λ /nm	ε /10^3 M^{-1} cm^{-1}	λ /nm	ε /10^3 M^{-1} cm^{-1}
580	10.1						
550	8.67	497	8.35	484	10	451	8.9
369	30.4						
308	10.1	353	25.4	319	12	314	11
276	10.4	272	11.6				
580	10.1						

The p*K*a values of ACCbs and ACSYCbs could not be determined accurately because of a competing reaction at high pH, the rate of which increased with increasing pH and temperature. The UV−vis spectra of ACCbs before and after this reaction took place are very similar, except for a small dilution effect. There is first a shift with increasing pH to a species whose $\alpha\beta$ and γ bands are at longer wavelength, as expected for cyanohydroxocobester. This shift then ceases at pH about 10.6 and, on allowing to stand overnight at pH greater than about 10.6, reverses itself. A similar effect was noted for ACSYCbs, but became noticeable at a slightly lower pH (about 10.2). Since the product has a UV−vis spectrum very similar to that of $[CN-Co[Cor]-OH_2]^+$ but a much higher pK_a, this reaction is ascribed to hydrolysis of one or more of the ester side-chains. Although acid hydrolysis is usually used to prepare cobesters with some carboxylic acid side-chains (for example[57]), a recent report describes the complete hydrolysis of dicyanocobester to give aquacyanocobyrinic acid (with 7 carboxylic acid side chains) using aqueous sodium hydroxide followed by neutralization with HCl.[58] A similar hydrolysis reaction was observed by Hamza for diaquacobester.[59]

An attempt was made to determine the pK_a for ACCbs by dissolving it in sodium phosphate buffer pH 8.00, μ = 0.1 M at 10.0 °C, and adding very small amounts of solid sodium hydroxide. By working rapidly we could *estimate* that the pK_a of ACCbs ~11. We attempted to determine the pK_a of ACSYCbs in a similar manner. Hydrolysis was found to occur at pH > 10.2 in this case, and since the spectral changes up to this pH are very small, we were unable to obtain even an estimate; the value is probably slightly less than that of ACCbs.

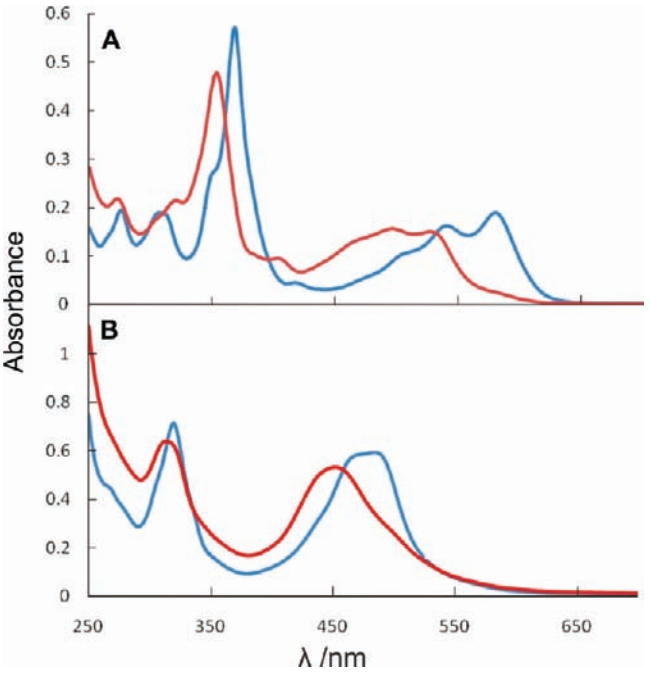

Figure 2. UV−vis spectra of (A) 1.88 × 10^{-5} M DCCbs (blue) and ACCbs (red) and (B) 6.0 × 10^{-5} M DCSYCbs (blue) and ACSYCbs (red), phosphate buffer, pH 8, μ = 0.1 M.

RESULTS

CD Spectra. During the preparation of DCCbs, epimerization at the C13 position could occur in acid solution[60,61] as seen in the X-ray crystal structures of CN-13-epiCbl.[62,63] The CD spectrum of DCCbs (Figure S1) is virtually identical to that reported previously for DCCbs in the same solvent,[64] and there is no indication of any C13 epimer which has a very different CD spectrum.[61] Epimerization does not occur under our conditions, and it seems likely that amide side-chains (as in cyanocobalamin) are necessary for epimerization.[61,64]

UV−Vis Spectra. The UV−vis spectra of DCCbs, ACCbs, DCSYCbs, and ACSYCbs are given in Table 2 and Figure 2, and the Gaussian deconvolution for DCCbs and DCSYCbs in Figure 3 and Table S1.

IR Spectra. The IR spectra of solid samples of DCCbs, ACCbs, DCSYCbs, and ACSYCbs are given in Table S2. All the cobesters show the presence of a small amount of water, which is consistent with the presence of water of crystallization seen in the crystal structure of DCSYCbs. The C═O stretch from the ester occurs at 1726−1730 cm^{-1}; the C═O lactone stretch appears at higher frequency (1780 cm^{-1}) in both DCSYCbs and ACSYCbs. The C≡N stretch occurs at 2123 cm^{-1} in DCCbs and at 2136 cm^{-1} in DCSYCbs. When the samples were dissolved in 1-butanol, there were very minor changes, with υ_{CN} shifting to 2124 cm^{-1} in DCCbs and to 2134 cm^{-1} in DCSYCbs.

Mass Spectrometry. The four cobesters studied in this work were examined using MS-FAB or MS-ESI. The molecular ions were expected at: DCCbs $C_{54}H_{73}CoN_6O_{14}$ (1088.45); ACCbs $C_{53}H_{75}CoN_5O_{15}$ (1080.46); DCSYCbs $C_{53}H_{71}CoN_6O_{15}$ (1090.43); and ACSYCbs $C_{52}H_{73}CoN_5O_{16}$ (1082.44). The mass spectra for each compound are given in the Experimental Section. In all cases M^+ was either not observed or was a low intensity peak. Even using mild ionization conditions, the loss of one or more of the axial ligands from the metal is facile. All four cobesters showed peaks consistent with the loss of one or both axial ligands, and also loss of an acetic acid methyl ester, as has been reported.[65]

Solid State Structure of DCSYCbs. Like many cobalt corrins,[66,67] the cobester crystallized in the orthorhombic space group $P2_12_12_1$ (R_1 = 6.08%, Figure 4) with Z = 4 (Figure S2); included in the unit cell is one methanol solvent molecule and one water molecule per cobester. The cobesters pack in chains along the crystallographic *a* axis (Figure S3) with each cobester connected by hydrogen bonding through methanol solvent molecules

dx.doi.org/10.1021/ic200285k |*Inorg. Chem.* 2011, 50, 8700–8718

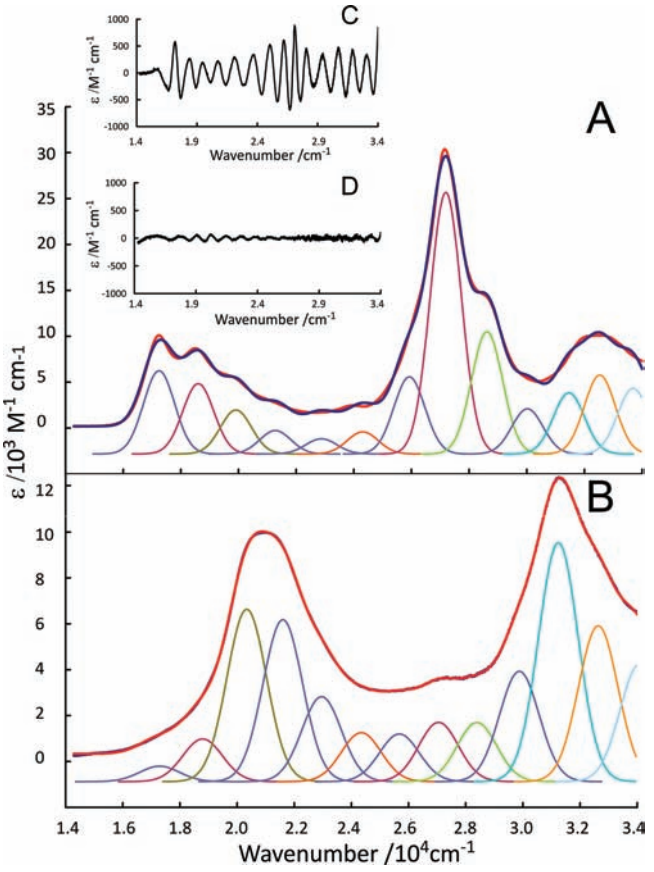

Figure 3. Gaussian deconvolution of the UV−vis spectrum of (A) 1.88×10^{-5} M DCCbs in phosphate buffer pH 8, $\mu = 0.1$ M and excess KCN, and (B) 1.62×10^{-5} M DCSYCbs in deionized water and excess KCN. The blue line is the experimental spectrum; the red line is the sum of the component Gaussian functions. The residuals are shown in parts C and D, respectively.

(*vide infra*). Pairs of chains are interlaced (Figure S4). Methanol acts as hydrogen bond donor to the β cyanide ligand (OH···NC 2.06 Å) and as hydrogen bond acceptor from the C5 hydroxyl group of a neighboring cobester (OH···OC 1.84 Å). The water molecule is hydrogen bonded to the α cyanide ligand (OH···NC 2.06 Å) and weakly hydrogen bonded to a neighboring cobester (OH···OC 2.415 Å).

A hydroxyl group has been added at the C5 position and is equatorial so that the C36 methyl group is axial, pointing toward the α face of the corrin; the absolute configuration at C5 is *R*. The *c* side chain forms a lactone at C6 oriented toward the β face (absolute configuration at C6 is *R*). The loss of the double bond between C5 and C6 has caused elongation of the bond. The average C5−C6 bond length in cobalt corrins that retain the double bond is 1.37(4) Å (from an interrogation of the Cambridge Structural Database, CSD[68]); here, the bond length is 1.520(8) Å. The C4−C5 bond is also somewhat elongated (1.506(8) Å), although nearly within 2σ of the CSD mean (1.45(3) Å). The C5−C35 bond length is normal (1.551(7) Å, cf. 1.53(3) Å in the CSD). The C4−C5−C6 valence angle is ideally tetrahedral, 109.2(5)°, compared to the mean trigonal value of 121.7(1.5)° for normal corrins in the CSD. Selected bond lengths and valence angles are listed in Table S3.

NMR Spectroscopy. ^{1}H and ^{13}C NMR assignments were made using the strategy previously described.[69] Despite the spectral crowding in the methylene (seven resonances between 29.7 and 32.9 ppm) and downfield (10 resonances between 172.0 and 176.8 ppm) regions of the ^{13}C spectrum, all ^{1}H and ^{13}C resonances could be unambiguously assigned (Table 3) save two of the ester methyl groups. The correlation table on which the assignments are based is given in the Supporting Information (Table S4). These assignments (and chemical shifts) agree precisely with the partial assignments previously made by Grüning et al.[35]

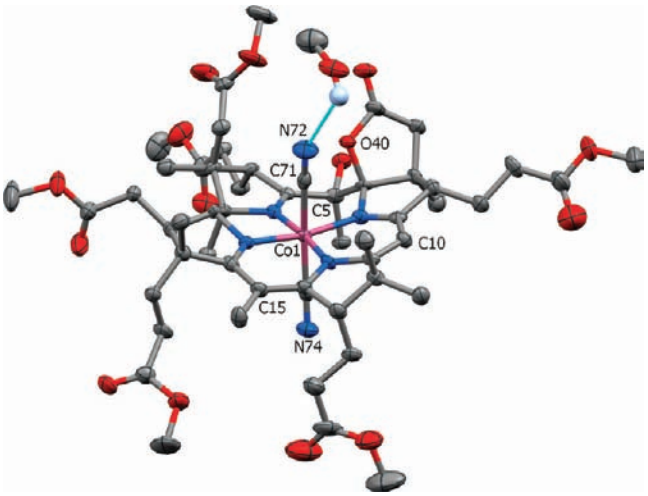

Figure 4. Asymmetric unit of the crystal structure of DCSYCbs. H atoms not involved in H-bonding and most atom labels are omitted for clarity. Some selected and standard labels (Figure 1) are placed to assist with visualization. Thermal ellipsoids are rendered at the 50% probability level.

In the 150 MHz 1D ^{13}C NMR spectrum, all six of the ester methyl resonances are resolved between 51.68 and 52.68 ppm, but in the 800 MHz ^{1}H spectrum, only five ester methyl group resonances appear between 3.64 and 3.78 ppm, with the resonance at 3.75 ppm having twice the integral of the other four resonances. Thus, unambiguous assignment of all six of the ester methyl resonances is impossible, even at 800 MHz. None of the ester methyl hydrogens had any NOE correlations with any other protons in the molecule in the ROESY spectrum, but each of the ester methyl groups has a three-bond correlation in the HMBC spectrum with the appropriate ester carbonyl carbon, with the ester methyl resonance at 3.75 ppm having correlations to two carbonyl carbons (at 52.09 and 52.41 ppm). As the ester carbonyl carbons were readily assigned by their two- (and sometimes three-) bond correlations with the side chain methylene protons, all of the ester methyl groups could be unambiguously assigned save for the *a* and *d* methyl esters.

The ^{13}C signals from the axial cyanide ligands of DCCbs (Figure 5) are broadened by the quadrupole moment and electric field gradient (EFG) of the Co(III) ion such that no ^{13}C−^{59}Co spin−spin coupling is resolved. Despite their low intensity and broadened line-shapes, the axial ligand resonances are clearly independently evident at 130.3 and 130.7 ppm in the ^{13}C NMR spectrum of DCCbs recorded at 30 °C. The ^{13}C signals for the axial ligands of DCSYCbs are similarly broadened. However, the ^{13}C nuclei are magnetically more dissimilar in this compound than in DCCbs, as reflected by the larger chemical shift difference (5.2 ppm) between the two resonances (129.1 and 134.3 ppm).

The ^{59}Co resonance of DCCbs was observed at 4074 ppm with a line width of 28 373 Hz (Figure 6). The chemical shift of the metal nucleus has previously been reported to occur at 4095

dx.doi.org/10.1021/ic200285k |*Inorg. Chem.* 2011, 50, 8700–8718

Table 3. ^{1}H and ^{13}C NMR Assignments for Dicyano Stable Yellow Cobester (DCSYCbs)[a]

group	$\delta 13_C$/ ppm	$\delta 1_H$/ ppm	group	$\delta 13_C$/ ppm	$\delta 1_H$/ ppm
C53	14.96	2.17	*d*-OCH_3	52.09 or 52.41	3.75
C25	16.05	1.26	*b*-OCH_3	52.68	3.78
C36	17.32	1.45	C13	53.47	2.92
C54	18.43	1.23	C8	55.91	2.83
C47	20.06	1.29	C17	58.44	
C20	21.75	1.43	C3	58.58	3.79
C41	22.29	1.94, 2.16	C19	76	4.25[b]
C30	22.88	2.08, 2.32	C5	79.04	
C35	23.55	1.88	C1	84.8	
C48	25.75	1.85, 2.06	C10	85.54	5.1
C56	29.71	2.25, 2.57	C5−O*H*		5.31
C46	30.71	1.14	C15	100.74	
C49	31.04	2.37, 2.64	C6	111.97	
C31	31.7	2.60, 2.70	*β*-CN	129.1[c]	
C60	31.85	2.47, 2.61	α-CN	134.3[c]	
C42	32.47	2.54	C14	164.6	
C55	32.87	1.73, 2.40	C61	171.98	
C18	39.88	2.86	C27	172.14	
C26	40.55	2.34, 2.94	C38	172.61	
C37	45.35	2.63, 2.93	C43	172.81	
C2	45.48		C57	173	
C12	46.69		C50	174.07	
C7	50.69		C16	174.32	
g-OCH_3	51.68	3.67	C32	175.47	
e-OCH_3	51.83	3.64	C11	175.64	
f-OCH_3	51.91	3.7	C9	176.82	
a-OCH_3	52.09 or 52.41	3.75	C4	191.19	

[a] In $CDCl_3$. Chemical shifts are relative to internal TMS. The designations *a*, *b*, etc. refer to the standard side chain lettering (see Figure 1). [b] J_{HH} = 10.4 Hz. [c] Assignment based on DFT-calculated ^{13}C magnetic shielding tensors.

ppm.[70] The resonance in DCSYCbs is shifted downfield to 4298 ppm and has a line width of 37 067 Hz.

DISCUSSION

Structure of DCSYCbs. As unambiguously established by X-ray crystallography (Figure 4), the reaction of DCCbs with ascorbate in the presence of O_2 oxidizes the C5 carbon with the addition of OH while the *c* side-chain forms a lactone at C6, presumably through a $[Co^{2+}O_2 \leftrightarrow Co^{3+}O_2^{-}]$ intermediate.[35] The crystal structure of DCSYCbs seems to be similar to that previously reported,[34] but the coordinates of that structure have not been deposited in the CSD, precluding any detailed comparison. An examination of the C−C and C−N bond lengths of the corrin (Figure S5) clearly shows that the conjugated system of a normal corrin has been interrupted between C5 and C6; there is an isolated double bond between N21−C4 and a triazamethine system with four conjugated double bonds between N22 and N24.

There are three reports of the crystal structure of DCCbs;[43,71,72] all three are of similar quality (R_1 = 10−13%). We have chosen the most recent structure[43] for comparison with our structure of DCSYCbs. Figure 7 shows an overlay of the crystal structures

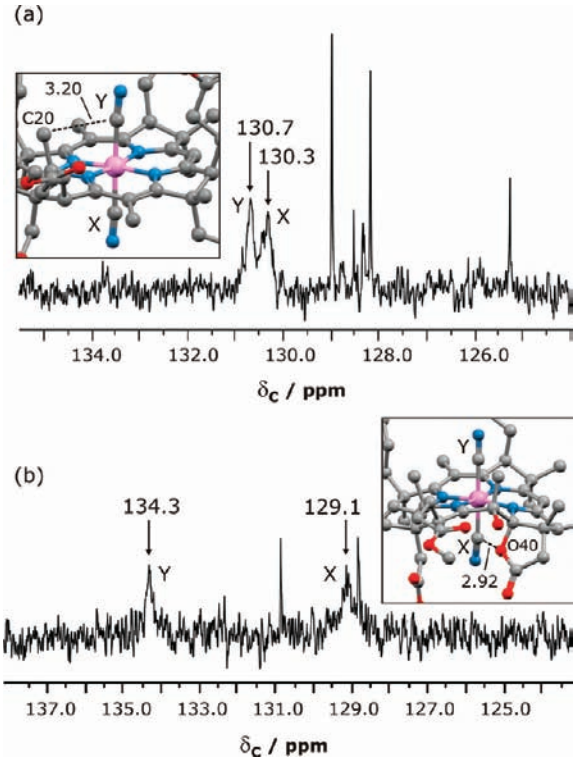

Figure 5. Expansion of the 130-ppm region of the ^{13}C NMR spectra of (a) DCCbs and (b) DCSYCbs recorded at 30 °C in $CDCl_3$. Signals from the axial cyanide ligand carbon atoms are highlighted. Key short nonbonded contacts (in Å) between the axial ligand carbon atoms and those of the macrocycle from the DFT-calculated structures are given in the insets to the spectra. (Atom numbering reflects the crystallographic numbering scheme.) Assignments were made from the isotropic component of the DFT-calculated magnetic shielding tensors for the relevant nuclei. (X = *β*-CN^- ion; Y = α-CN^- ion.).

of DCSYCbs and DCCbs.[43] A comparison of the bond lengths and valence angles of the corrin core of the two structures is given in Table S5. The structure of DCCbs is significantly poorer than the present structure of DCSYCbs (R_1 = 11.46% and 6.08%, respectively) so caution is needed when comparing the two structures. Bond lengths differ by about 0.02 Å on average, which is within the uncertainty of the bond lengths in DCCbs. The notable exception is the C5−C6 bond which increases from 1.33(2) Å in DCCbs to 1.520(8) Å in DCSYCbs, consistent with the loss of double bond character.

Valence angles are, on average, within 1° of each other, with the exception of the C4−C5−C6 angle (109.2(5)° in DCSYCbs and 122(1)° in DCCbs) and the C5−C6−N22 angle (114.2(4)° and 126(1)°, respectively) due to addition of OH to C5 and formation of the lactone at C6. The C20−C1−N21 angle is significantly smaller in DCSYCbs (106.3(4)°) than in DCCbs (114(1)°), but the reason is not obvious.

The Co−CN(*β*) bond length (1.931(6) Å) in DCSYCbs is somewhat longer than the Co−CN(α) bond (1.918(6) Å), although the difference is within the sum of the uncertainties of the two measurements. An examination of six crystal structures of dicyano cobesters (three of DCCbs itself,[43,71,72] one in which the *a* and *c* amides are preserved,[73] one in which the *b* side chain is the free acid,[57] and the norcobyrinic acid derivative where the C15 methyl is missing[74]) shows that Co−CN(α) is always, but

dx.doi.org/10.1021/ic200285k |*Inorg. Chem.* 2011, 50, 8700–8718

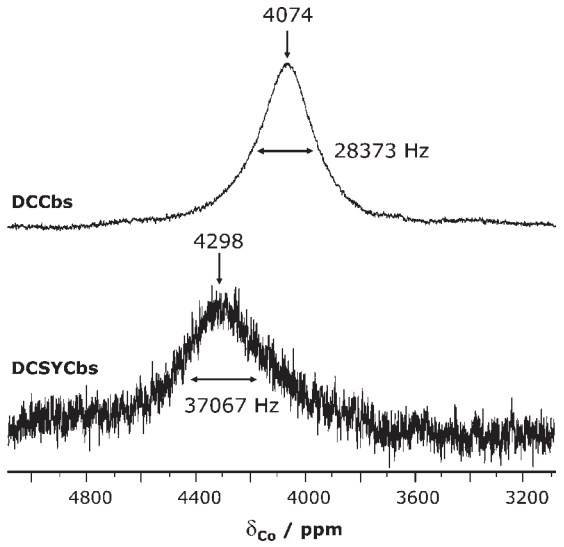

Figure 6. ^{59}Co NMR spectra of DCCbs and DCSYCbs recorded in $CDCl_3$ at 30 °C. The chemical shift and line width parameters shown are from deconvolution of the spectra (40% Gaussian−Lorentzian functions). Estimated standard errors of the fit parameters are <0.2%.

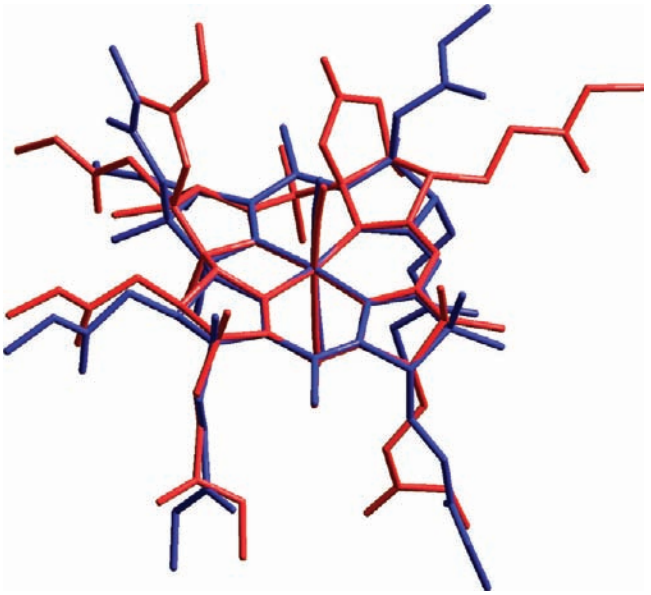

Figure 7. Overlay at the four corrin N's and Co of the crystal structure of DCSYCbs (red) and that of DCCbs (blue).

only very marginally, longer than Co−CN(β) (by 0.013 ± 0.017 Å). So the slightly longer Co−CN(β) in DCSYCbs may reflect the steric influence of the *c*-lactone.

There are two structures related to DCSYCbs where the *c* side chain forms a lactam at C6. In 5,6-dihydro-5-hydroxy-heptamethylcob(III)yrinate-*c*,6-lactam,[35] the Co−CN(β) bond length is 1.955(9) Å and definitely longer than the Co−CN(α) bond length (1.899(9) Å). In the two molecules in the unit cell of 5,6-dihydro-hexamethylcob(III)yrinate-*a*-amide-*c*,6-lactam,[75] the Co−CN(β) bond lengths (1.9509(8) Å and 1.9260(8) Å) are also longer than the Co−CN(α) bond lengths (1.947(1) and 1.891(1) Å). The corrin fold angle (the angle between the mean planes through N21, C4, C5, C6, N22, C9, and C10—plane 1—and through N24, C16, C15, C14, N23, C11 and C10—plane 2—respectively[76]) in DCSYCbs is 15.7° but only 5.2° in DCCbs. This might be a contributory factor to the elongation of the Co−CN(β) bond length; however, since in the two molecules in the unit cell of 5,6-dihydro-hexamethylcob(III)yrinate-*a*-amide-*c*,6-lactam the fold angles are only 5.9° and 6.0°, an increased corrin fold angle does not appear to be a significant factor contributing to the elongation of the Co−CN(β) bond.

The NC−Co−CN angle in DCSYCbs is 173.0(2)° and the two CN^- ligands are bent away from the "western" toward the "eastern" half of the molecule, and not, significantly, away from O40 of the *c*,6-lactone (see Figure 1 for numbering). Such a distortion is common in all the dicyano complexes referred to above, and there is no difference in the distortion of the *trans* axial bond between normal corrins and those with a lactam or lactone at C6. The distortion appears to originate from a close contact of C19H and the C20Me with the β ligand (Figure 8).

NMR Spectroscopy. Several groups have reported the ^{13}C and ^{1}H NMR assignments of Co(I)-DCCbs,[77] Co(III)-DCCbs,[78−81] and the Co(III)-DCCbs-monoacids[57] and -monoamides.[79] Ernst notes a single value for the ^{13}C resonance of the two coordinated cyanide ligands in DCCbs, at approximately 130 ppm ($CDCl_3$) or approximately 133 ppm (CD_3OD),[78] and subsequently[79] at 130.0 ppm ($CDCl_3$). In the case of the *b*-, *d*-, *e*-, and *f*-monoamide-hexamethylesters, two ^{13}C resonances were reported for the axial cyanide ligands differing by as little as 0.6 ppm in the *b*-monoamide, to at most 4.7 ppm in the *e*-monoamide (133.9 and 129.2 ppm). The resonances were not assigned to a particular ligand of each diastereomer. In the case of the monoacids,[57] two resonances were observed, with differences ranging from 0.63 ppm (130.59 and 131.22 ppm) for the *b*-monoacid to 4.05 ppm (129.93 and 133.38 ppm) for the *e*-monoacid. In this case the authors tentatively assigned the downfield resonance to the α-CN ligand.

In our ^{13}C NMR spectrum of DCCbs (Figure 5a, $CDCl_3$) we found the two cyanide resonances at 130.69 and 130.29 ppm, consistent with their similar magnetic and chemical environments, as evidenced by the X-ray structure of the compound which has identical Co−C axial bond distances (1.92(1) and 1.92(2) Å, respectively). The marginal difference in their chemical shifts were confirmed by *in vacuo* DFT simulations (*vide infra*). However, the C of the α-CN^- ion (Y ligand, Figure 5a) makes a short contact (3.20 Å) with C20 and may therefore be distinguished magnetically from the β-CN^- ion (X ligand), a distinction that is not only experimentally observed in the ^{13}C NMR spectrum, but is also apparent in the DFT-calculated magnetic shielding tensors (*vide infra*) for the axial ligand carbon atoms. We have therefore assigned the downfield ^{13}C resonance (130.69 ppm) to the α-CN^- ion based on the smaller calculated isotropic shielding constant for this ligand carbon atom (Table 4).

The axial cyanide ions of DCSYCbs are also magnetically unique by virtue of their location within dissimilar ligand binding pockets of the Co(III) macrocycle, as evidenced by the well-separated signals at 129.1 and 134.3 ppm (Figure 5b). These signals are in the same general chemical shift range as the cyanide ions of DCCbs and are similarly broad due to coordination of the carbon atoms to the Co(III) ion with its large nuclear quadrupole moment. As shown in Figure 8, the axial cyanide ion coordinating on the β-face (X ligand) of the macrocycle experiences greater steric restriction than that coordinating on the α-face (Y ligand), accounting for its slightly larger off-axis tilt. From the DFT-calculated

dx.doi.org/10.1021/ic200285k |*Inorg. Chem.* 2011, 50, 8700–8718

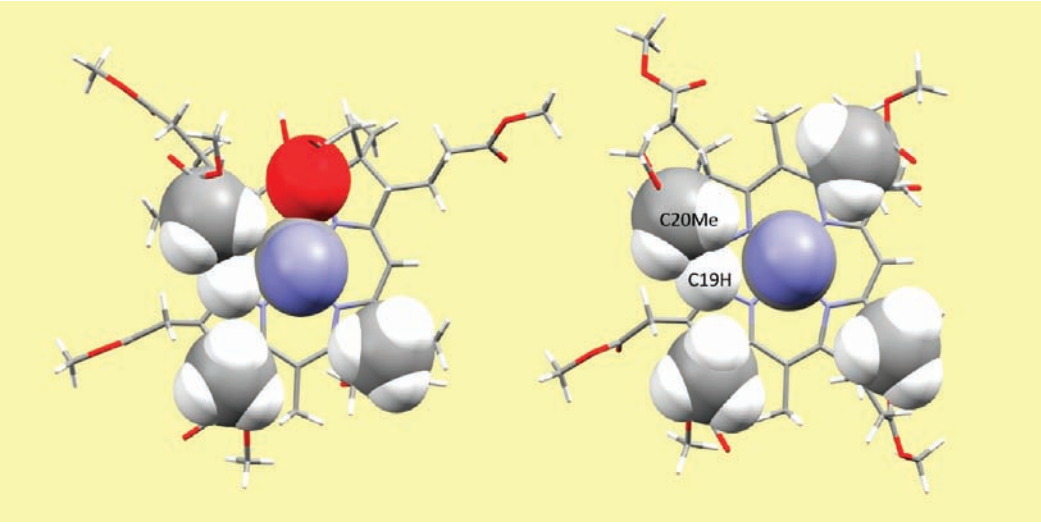

Figure 8. View of the β face of (left) DCSYCbs and (right) DCCbs. The sentinel C46 and C54 methyl groups, the C19 proton, O40 of the *c*,6 lactone of the SYCbs, and the C37 methylene group of the Cbs are drawn with a space-filling model using the standard van der Waals radii of these atoms. Formation of the *c*,6-lactone brings O40 into the ligand binding pocket of the β face of the corrin (left). Although located largely over C5, O40 does make van der Waals contact with the C-donor atom of coordinated cyanide.

Table 4. Selected Magnetic Shielding Tensors for DCCbs and DCSYCbs Calculated Using DFT-GIAO Methods at the PBE1PBE/6-311G Level of Theory[a,b]**

	σ_{iso}/ppm	η/ppm	σ_{xx}/ppm	σ_{yy}/ppm	σ_{zz}/ppm	δ_{Co}^{calc}/ppm	δ_{Co}^{exp}/ppm[c]	Δ/ppm
				DCCbs				
Co	−10 282.0	1207.7	−9927.7	−9888.8	−11 029.5	3659.8		
Co ($CHCl_3$)	−10 221.4	1121.3	−9904.4	−9899.1	−10 860.8	3573.7	4074	−500.3
Co (MeOH)	−10 185.4	1060.0	−9894.0	−9916.3	−10 745.8	3530.2		
β-CN (X)	35.6	330.8	−26.7	−52.5	185.9	153.9	130.3	23.6
α-CN (Y)	32.2	333.7	−35.4	−44.8	177.0	157.2	130.7	26.6
C-20	164.9	13.7	167.4	158.7	168.4	24.6	22.1	2.6
C-25	170.3	13.9	164.2	177.0	169.5	19.2	17.0	2.3
				DCSYCbs				
Co	−10 272.2	1229.0	−9912.8	−10 059.1	−10 844.6	3650.0		
Co ($CHCl_3$)	−10 218.9	1115.0	−9903.6	−10 058.9	−10 694.2	3571.1	4298	−726.9
Co (MeOH)	−10 185.7	1054.9	−9909.3	−10 057.8	−10 590.0	3530.5		
β-CN (X)	34.0	329.4	−70.7	−54.6	227.2	155.5	129.1	26.4
α-CN (Y)	28.5	337.1	−44.3	−25.9	155.6	161.0	134.3	26.7
C-20	165.3	16.3	173.5	148.7	173.6	24.2	21.8	2.5
C-25	172.3	18.5	171.5	176.1	169.3	17.2	16.1	1.1

[a] Nonstandard symbols: η, asymmetry parameter; Δ, chemical shift difference ($\delta_{Co}^{exp} - \delta_{Co}^{calc}$); atom numbering follows that given in Figure 1. [b] Calculated shielding parameters are for the gas phase complexes unless otherwise indicated. [c] Experimental chemical shifts were measured in $CDCl_3$.

magnetic shielding tensors for the Co(III)-bound axial carbon atoms (Table 4), the β-CN^- C is more shielded than that of α-CN^-. The resonances at 129.1 and 134.3 ppm in the ^{13}C NMR spectrum of DCSYCbs are therefore assigned to the β- and α-CN^- ions, respectively.

We found no observable long-range proton couplings to the axial CN^- in DCSYCbs. The axial ligand ^{13}C resonances of dicyanocobinamide (DCCbi) have been reported at 140.60 and 141.60 ppm.[82] The separation of the two resonances, $\Delta\delta_C^{ax}$, in DCSYCbs (5.08 ppm) is much larger than that in DCCbi (1.00 ppm) or in DCCbs (0.40 ppm). The *in vacuo* DFT-calculated chemical shift differences between the α- and β-CN^- ^{13}C resonances of DCCbs and DCSYCbs were 3.3 and 5.5 ppm, respectively, in good agreement with the experimental $\Delta\delta_C^{ax}$ values. The large axial ligand chemical shift difference in DCSYCbs does not arise because of differences in the Co−C bond lengths; the experimental (X-ray) values are in fact equivalent within 1σ and the *in vacuo* DFT-calculated Co−C distances are identical (1.927 Å). The origin of the large $\Delta\delta_C^{ax}$ value is therefore most likely due to the difference in tilt of the two axial ligands (*vide supra*) and their nonequivalent local environments.

dx.doi.org/10.1021/ic200285k |*Inorg. Chem.* 2011, 50, 8700–8718

Some of the difference between the cobesters and the cobinamide is attributable to the difference in bulk magnetic susceptibility of the solvents used in the measurements ($CDCl_3$ for DCSYCbs and DCCbs, and D_2O for DCCbi, *vide infra*), but both resonances are still significantly shifted downfield in the cobinamide. This reflects a significant difference in electronic interaction between the cyanide ligands and the metal in the two cobesters compared to DCCbi (although a much smaller difference between DCCbs and DCSYCbs).

Despite the difference in solvent ($CDCl_3$ for DCSYCbs and D_2O for DCCbi[83]), a comparison of the ^{13}C chemical shifts between DCSYCbs and DCCbi is still instructive (Table S6). Included are other available ^{13}C chemical shift data for DCCbs itself reported by others[79,81] and data which we have recorded and assigned by analogy. We also list in Table S6 the ^{13}C resonances of a compound related to DCSYCbs, Coα,Coβ-dicyano-5,6-dihydro-pentamethylcob(III)yrinate-*a*-amide-*c*,6-lactam, DCLCbs,[84] in which the corrin is reduced at the C5−C6 bond and contains a *c*,6 lactam, and the amide of the *a* side chain is retained. Although the ^{13}C chemical shifts are reported, they have not been completely and unambiguously assigned. We have tentatively assigned them on the basis of the assignments for DCCbi.[83]

The average change in ^{13}C chemical shift of the resonances of the corrin ring carbons which are remote from the structural alterations in DCSYCbs and unaffected by the changes in resonance conjugation in the corrin ring (i.e., C1−C3, C11−C19 inclusive, $n = 12$) is an upfield shift of 2.8 ± 1.7 ppm in DCSYCbs compared to DCCbi, evidently due to the difference in bulk magnetic susceptibility of the two solvents. The analogous differences between DCSYCbs and DCCbs are very small ($|\Delta\delta| = 0.9 \pm 0.7$ ppm for the two spectra of DCCbs reported[79,81] together with the spectrum we recorded), as is the case for DCLCbs ($|\Delta\delta| = 0.8 \pm 0.8$ ppm). A similar trend is observed for the methyl resonances of the corrins (i.e., C20, C25, C47, C48, C53, C54), with $\Delta\delta = -2.3 \pm 0.7$ ppm for DCCbi, $|\Delta\delta| = 0.4 \pm 0.5$ for DCCbs, and $|\Delta\delta| = 0.2 \pm 0.2$ ppm for DCLCbs ($n = 6$).

The conversion of the side chain amides to methyl esters results in an upfield shift of 6 ± 1 ppm of the carbonyl carbon chemical shifts ($n = 5$, excluding C43), and an upfield shift of 4.4 ± 1.1 ppm on the chemical shift of the side chain methylene carbon adjacent to the carbonyl ($n = 5$, excluding C42). There is little difference in these resonances between DCSYCbs and DCCbs, with the exception of the *b*-side chain resonances where C32 resonates 2.55,[79] 2.48,[81] and 2.56 ppm (this work) upfield while C31 resonates 2.11[79,81] and 2.02 ppm (this work) downfield for reasons that are not obvious.

Much larger effects are caused by the hydroxylation at C5 and the cyclization of the *c*-side chain with the B ring. Compared to DCCbi, these structural changes shift the C5 and C6 resonances upfield by 28.8 and 53.7 ppm, respectively, consistent with a change in hybridization of these C atoms. The C4 resonance moves downfield by 11.7 ppm, presumably because interruption of the conjugation allows greater polarization of the N21−C4 electron density toward N. The effects are negligible, however, on C7 and C8 (1.1 and 2.0 ppm upfield, respectively). A comparison of the ^{13}C resonances of DCSYCbs and DCCbs shows very similar effects. Using an average of the three reports (this work and refs 79 and 81) of the ^{13}C resonance data for DCCbs, we find $\Delta\delta = -24.6$ and -51.6 ppm for C5 and C6, respectively, +15.8 ppm for C4, and a negligible +2.0 and 1.7 ppm for C7 and C8, respectively.

The C5 resonance of DCCbs (41.3 ppm) is 37.7 ppm upfield compared to that of DCSYCbs (the effect of H− compared to HO− substitution at C5), and the C6 resonance (90.6 ppm) is 21.4 ppm upfield (the weaker inductive withdrawing effect of the lactam compared to the lactone). The *c*-side chain cyclization causes a surprising 7.0 ppm upfield shift of the C41 methylene resonance (compared to DCCbi; 4.2 ppm compared to DCCbs), and a 4.1 ppm upfield shift of the C36 methyl resonance (2.0 ppm compared to DCCbs).

The ^{59}Co chemical shifts help shed some light on the nature of the metal in the two compounds. The ^{59}Co resonances of CNCbl, AdoCbl, and MeCbl in aqueous solution have been reported to occur at 4650, 4480, and 4125 ppm.[70] Thus, as the donor power of the axial ligand and its interaction with the metal increases, the ^{59}Co resonance shifts upfield. A similar effect has been noted in the cobaloximes where replacement of H_2O *trans* to ethyl by strong donors such as imidazole or pyridine results in increased shielding of the ^{59}Co nucleus.[85] In the present study, the ^{59}Co resonance of DCCbs was observed at 4074 ppm while that for DCSYCbs was observed further downfield (4298 ppm). Since the DFT-calculated and crystallographically determined axial Co−C bonds are, within the errors of each method, equivalent for the two structures (Table S7), the experimental difference in the ^{59}Co chemical shift for the two complexes cannot be attributed to differences in the Co−CN bonding interactions and points to fundamental differences between the interaction of the Co(III) ion with the *cis* macrocycles in the present pair of compounds. Clearly, the more delocalized corrin π-electron system of DCCbs relative to that of DCSYCbs favors formation of a more covalent complex with the metal ion, accounting for the stronger shielding of the Co(III) core electrons.

Cyanide Stretching Frequencies. The CN^- ligand is unusual in that the frequency of its C≡N stretch *increases* on coordination to a metal ion.[86−88] As the donor power of the ligand *trans* to CN^- in a cobalt corrin increases, ν_{CN} decreases and may approach the stretching frequency of free cyanide (reported at between 2078 and 2080 cm^{-1});[89,90] for example, ν_{CN} = 2130, 2119, 2088, and 2083 cm^{-1} in cobalt corrins where the *trans* ligand is H_2O, CN^-, methyl, and *n*-propyl, respectively.[91] In early work performed by one of us,[92] an inverse relationship between $\delta^{15}N$ and $\delta^{13}C$ in the NMR of ^{15}N- and ^{13}C-labeled coordinated CN^- in some cobalamins was found and attributed to a significant contribution of a resonance structure $Co^+{=}C{=}N^-$, arising from dπ−pπ metal-to-ligand back-bonding. This model was then used to explain the observed variation in ν_{CN} of cyanocobaloximes, $CNCo(dmgH)_2L$, with variation in the σ donor power of the *trans* ligand L (assessed from the pK_a value of its conjugate acid).[93] As the pK_a of L increased for a series of pyridines, anilines, and primary amines, ν_{CN} shifts to lower values while, in parallel, $\delta^{13}C$ shifted downfield and $\delta^{15}N$ shifted upfield.

There is also evidence for the *cis* influence of the macrocycle. For example, ν_{CN} in *trans* dicyanides [CNCo(L)CN] occurs at 2119 cm^{-1} for L = corrin,[94] 2124 cm^{-1} for L = octaethylporphyrin,[95] 2130 cm^{-1} for L = cobaloxime,[96] and 2134 cm^{-1} for L = [14]aneN$_4$,[97] in exact parallel to the kinetic *cis* effect referred to in the Introduction. We therefore expect that as the strength of the interaction between Co(III) and the equatorial macrocyclic ligand increases, ν_{CN} of axially coordinated CN^- will shift to lower frequency. We measured ν_{CN} of solid KCN at 2078 cm^{-1}. In DCSYCbs and ACSYCbs (2138 and 2137 cm^{-1} in the solid state, respectively; 2134 cm^{-1} for DCSYCbs in 1-butanol solution) ν_{CN} occurs at a higher frequency than in DCCbs and ACCbs, *viz.*,

2123 (2124 in 1-butanol) and 2129 cm^{-1}, respectively; hence, the corrin ligand in DCCbs interacts more strongly with the metal than does the stable yellow corrin ligand with its diminished conjugation.

Experimental UV−Vis Spectra. The UV−vis spectrum of DCCbs (in aqueous solution) is identical to that previously reported.[43] Gaussian deconvolution (Figure 3A) shows the α-band at 17 244 cm^{-1} (580 nm) followed by three bands with diminished intensity and equal spacing (1344 ± 32 cm^{-1}), D and E bands at 22 875 and 24 310 cm^{-1} (437 and 411 nm), and the γ-band at 27 191 cm^{-1} (368 nm) with two bands of lesser intensity on either side at 25 928 and 28 621 cm^{-1} (386 and 349 nm), respectively. The α-band and the three following bands, including the β-band, may represent a vibrational progression[98] of the HOMO to LUMO $\pi \rightarrow \pi^*$ electronic transition (see the DFT-calculated transitions and assignments below), but the two bands on either side of the γ-band appear to correspond to separate electronic transitions.

The UV−vis spectrum for DCSYCbs in aqueous solution and methanol is identical to that previously reported.[34] The spectrum shows similar features to that of DCCbs, except that all peaks are shifted to shorter wavelength and the γ-band is much less intense. Gaussian deconvolution (Figure 3B) shows that the α-band is at 20 337 cm^{-1} (492 nm) and is followed by four bands with diminished intensity and approximately equal spacing (1335 ± 53 cm^{-1}). Although it is tempting to speculate that these four bands are exclusively due to a vibrational progression (as in DCCbs), our DFT simulations (*vide infra*) indicate that the spectral region to the blue of the α-band is particularly complex and also includes several independent singlet electronic excited states unique to DCSYCbs. The D and E bands are at 27 049 and 28 392 cm^{-1} (370 and 352 nm), and the γ-band is at 31 241 cm^{-1} (320 nm), with two bands of lesser intensity on either side at 29 874 and 32 635 cm^{-1} (335 and 306 nm), respectively. In addition, there are two low-intensity peaks at longer wavelength than the α-band; these are absent in the gas phase DFT-calculated electronic spectrum of DCSYCbs and cannot be attributed to conventional singlet excited states of the chromophore. The ratio of the extinction coefficient of the γ-band to that of the α-band is 1.4, which is much less than the corresponding ratio (3.1) for DCCbs. The HOMO to LUMO $\pi \rightarrow \pi^*$ electronic transition corresponding to the α-band is shifted to higher energy (by 3100 cm^{-1}), due to the shorter delocalized system. The γ-band also shifts to higher energy to a slightly greater extent (by 4050 cm^{-1}) than the α-band. The shifts in energy and differences in intensity between DCSYCbs and DCCbs are similar to those observed by Eschenmoser[99] for two corrinoid precursors, with and without a break, respectively, in the conjugated system at C5.

DFT Calculations: The Choice of Methodology. Several recent DFT studies on simplified Co(III)-corrin derivatives, devoid of peripheral substituent groups, have suggested that the BP86 functional performs well, with a 6-31G(d) basis set, for structural accuracy and calculation of the singlet excited states using TD-DFT[100] for cyanocobalamins (CNCbl).[101−103] A close inspection of some of the results plotted in several of these reports, however, reveals that there are some significant shortcomings in electronic spectral predictions with the BP86 functional. For example, oscillator strengths (over the whole spectrum) and transitions in the UV region, especially for CNCbl model complexes, tend to give at best adequate and often rather poor matches of the experimental spectra, despite claims to the contrary that the BP86 functional fares better on average than hybrid DFT functionals such as B3LYP.[104] This is strikingly illustrated in a recent comparative study of the singlet excited states predicted by the BP86/aug-cc-pVDZ and CAM-B3LYP/aug-cc-pVDZ methods for a CNCbl model complex by the same authors,[105] which showed that the latter hybrid functional more accurately predicts the electronic spectrum of CNCbl (but not that of MeCbl). Appraisal of the literature on DFT simulations of structural geometries, spectra, shielding tensors, and many other electronic properties quickly reveals that there is no perfect combination of DFT functional and basis set, with all approaches having strengths and weaknesses (the latter becoming more prevalent with increasing system complexity). We elected to use the PBE1PBE hybrid functional with a large basis set because there is a good body of evidence for this functional affording some of the better system-independent geometry, NMR shielding tensor, and electronic spectral simulations.[106−111] While our goal in this paper is not to compare DFT methods, but to use a reliable DFT method to gain insight into the electronic structures of DCCbs and DCSYCbs, we nevertheless felt it necessary, and as recommended by a reviewer of this work, to check the performance of the BP86 functional for these compounds. The results are summarized in Table S7 and show that the PBE1PBE functional gives the more accurate geometry predictions (3-fold better mean bond deviations relative to the X-ray data). Moreover, this method allowed us to compute all other electronic structure parameters for the compounds of interest routinely (i.e., no wavefunction convergence failures or similar hallmarks of inadequate theoretical methods). In our hands, all BP86/6-311G(d,p) simulations on DCCbs and DCSYCbs were unsuccessful in the Gaussian 03 package, typically failing during 2-electron integral evaluation (frequency jobs and excited state determinations). This problem was manifest despite the use of ultrafine grids, more than ample random-access memory, and various SCF convergence schemes. In short, we have used a well-tested method that works for the untruncated structures of DCCbs and DCSYCbs in this study.

DFT Calculations: Shielding Tensors. Calculations at the PBE1PBE/6-311G(d,p) level of theory produced energy-minimized structures of DCCbs and DCSYCbs that are in good agreement with the crystal structures (mean bond lengths and valence angles to within 0.02 Å and 1.5°, respectively, of the experimental values; Table S7). An exhaustive analysis of all the calculated and observed shielding values (^{1}H, ^{13}C, ^{59}Co) for the two compounds, while potentially interesting, is beyond the scope of the present report. Some brief comments pertinent to the shielding data given in Table 4 are, however, warranted.

First, the ^{13}C chemical shifts for nuclei physically removed from the metal ion are accurately calculated to within 3 ppm and are in the correct relative order. Interaction of the ^{13}C nuclei of axial CN^- with the quadrupole moment of the ^{59}Co nucleus leads to line broadening in the experimental spectrum and a poor estimate of the ^{13}C isotropic shielding by the DFT method used (the predicted chemical shift is larger than the observed chemical shift by 20−30 ppm). The relative order of the calculated axial ligand chemical shifts, however, is likely to be more reliable. Second, the experimental ^{59}Co NMR line width reflects the magnitude of the asymmetry parameter, η, of the calculated shielding tensor for the nucleus (DCCbs has a narrower line width and smaller asymmetry parameter than DCSYCbs). Third, the calculated ^{59}Co chemical shifts are in poor agreement with the experimental chemical shifts (400−800 ppm upfield of the

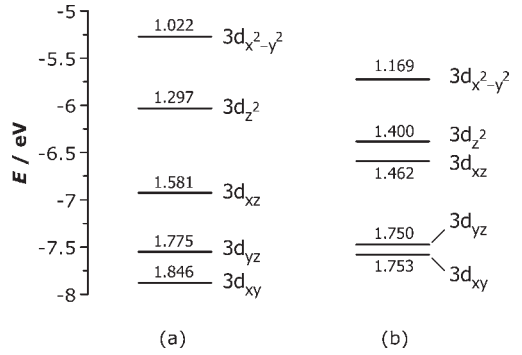

Figure 9. 3d orbital energies and NBO electron populations in (a) DCCbs and (b) DCSYCbs from a PBE1PBE/6-311G** calculation.

measured values). This problem is well-documented for GIAO DFT simulations for a range of metal nuclei[112−115] and, as indicated in Table 4, does not improve with inclusion of a solvent polarization continuum (e.g., methanol or chloroform) in the simulation. The large difference in the experimental ^{59}Co chemical shifts for DCCbs and DCSYCbs is not reproduced by the DFT calculations, which also incorrectly predict that DCCbs is marginally less shielded than DCSYCbs. On the basis of the above points, we conclude that GIAO-DFT, whether with the present hybrid functional and basis set or with the B3LYP hybrid functional[116,117] and a similarly large basis set augmented with f-orbital polarization functions,[118] is not particularly well suited for predictions of absolute and relative chemical shifts of heavier nuclei such as ^{59}Co. The method is, however, adequate (and in fact quite accurate) for lighter nuclei in conventional chemical and magnetic environments.

DFT Calculations: Electron Distributions. Figure 9 shows the natural bond orbital (NBO) 3d orbital energies and electron populations of the metal ion in the two compounds. While the total 3d orbital population (Table S8) is very similar (7.521 e in DCCbs and 7.534 e in DCSYCbs), the 3d orbitals in the former span a significantly greater energy range (2.61 eV) than in the latter (1.86 eV), consistent with greater overlap between the corrin and the metal orbitals, which gives the metal in DCCbs a softer, more covalent character. The 3d radial expectation values for the two complexes, $\langle r^{-3}\rangle_{3d}$, also reflect the degree of mixing of the atomic orbitals of the cobalt ions in their distinct coordination environments with the MOs of the corrin-type macrocycle in each case. Thus, DCCbs has a higher value of $\langle r^{-3}\rangle_{3d}$, 4.9678, compared with 4.9576 for DCSYCbs, presumably due to enhanced metal-to-corrin orbital overlap and electron density polarization.

Delocalization of metal electron density onto the macrocycle (the nephelauxetic effect) would be promoted by a more highly π-conjugated corrin macrocycle system. Inspection of the frontier MOs of the two complexes (Figure 10) strikingly confirms the diminished delocalization pathway for DCSYCbs and the likelihood that this macrocycle is intrinsically the harder of the two; this is confirmed by the HOMO−LUMO gap, which is 3.26 eV in DCCbs but larger in DCSYCbs (3.73 eV, Figure S6). A final consequence of enhanced equatorial M−L overlap in DCCbs is the transfer of electron density away from the [CoN_4] core: the net NBO charge for the [CoN_4] core in DCCbs (−0.975 e) is lower than that for DCSYCbs (−1.048 e, Table S8).

The NBO-calculated 4s atomic orbital electron density is 1.4% lower in DCSYCbs relative to DCCbs (Table S8). Because the 4s atomic orbital wavefunction has a nonvanishing amplitude at the nucleus, this drop in electron density would account for reduced shielding of the nucleus and could explain most of the downfield shift of the ^{59}Co NMR signal for DCSYCbs relative to DCCbs.

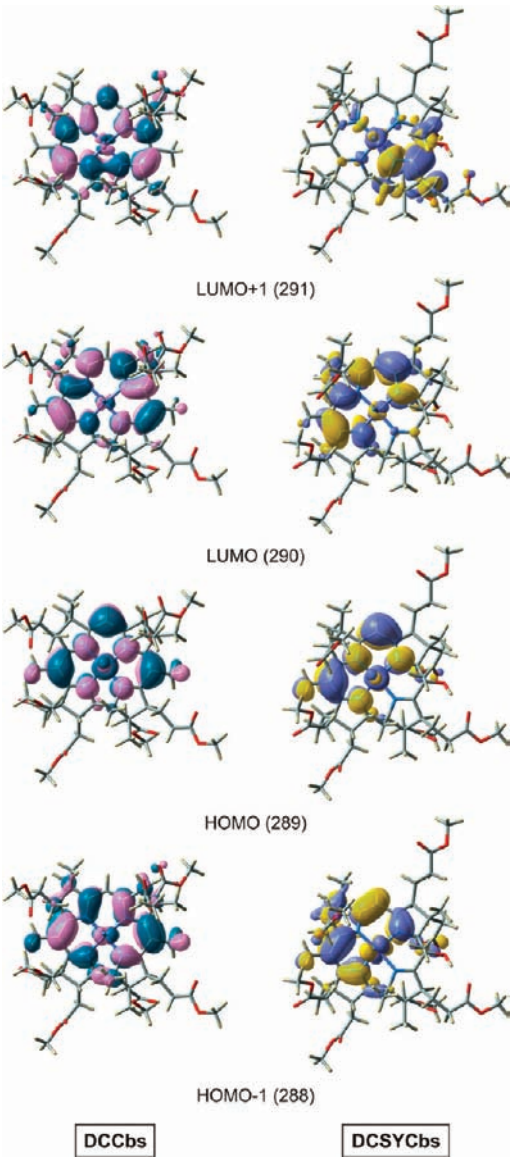

Figure 10. Comparison of the frontier molecular orbitals for DCCbs and DCSYCbs (PBE1PBE/6-311G** wavefunction).

DFT Calculations: Electronic Transitions. The experimental UV−vis spectra of DCCbs and DCSYCbs (Figure 2) are markedly different, and both are inherently complex due to the nature and low symmetry of the macrocycle coordinated to the Co(III) ion. Straightforward assignment of the principal transitions is therefore difficult, and numerous theoretical methods have been used over a period spanning more than four decades to delineate the spectra of vitamin B_{12} and its analogues.[31,119−122] In this work, we have deconvoluted the spectra of DCCbs and DCSYCbs into constituent Gaussian bands (Figure 3) to create a useful starting point from which a clearer picture of the key electronic transitions for each complex could be constructed using a time-dependent DFT (TD-DFT) simulation,[52] which is especially useful for understanding the orbital parentages of the electronic excited states for a chromophore. Implicit in our

dx.doi.org/10.1021/ic200285k |Inorg. Chem. 2011, 50, 8700–8718

Table 5. DFT-Calculated Excited Singlet States (*in Vacuo*) and Main Transition Assignments for DCCbs (TD-DFT Method, PBE1PBE/6-311G Level of Theory)[a,b]**

λ^c/nm	$\lambda^{s\,d}$/ nm	MOs	largest coeff	%	f^e	transition assignment
513.8	554.6	289 → 290	0.660	100	0.1189	$\pi \rightarrow \pi^*$
417.0	450.1	273 → 292	0.394	29.9	0.0010	$d_{xy} \rightarrow \sigma^*, d_{x^2-y^2}{}^*$
		288 → 292	0.288	21.9		$d_{xz}, \pi \rightarrow \sigma^*, d_{x^2-y^2}{}^*$
403.5	435.5	273 → 292	−0.264	17.6	0.0006	$d_{xy} \rightarrow \sigma^*, d_{x^2-y^2}{}^*$
		286 → 292	−0.261	17.4		$d_{xz}, \pi(CN) \rightarrow \sigma^*, d_{x^2-y^2}{}^*$
400.5	432.3	270 → 292	0.316	21.5	0.0010	$d_{yz}, \pi \rightarrow \sigma^*, d_{x^2-y^2}{}^*$
		288 → 293	−0.226	15.3		$d_{xz}, \pi \rightarrow \pi^*, d^{z^2}, \sigma^*(CN)$
377.0	406.9	289 → 291	0.563	51.5	0.0027	$\pi \rightarrow \pi^*, d_{x^2-y^2}{}^*$
		288 → 290	0.374	34.2		$d_{xz}, \pi \rightarrow \pi^*$
356.3	384.5	289 → 292	0.511	48.9	0.1142	$\pi \rightarrow \sigma^*, d_{x^2-y^2}{}^*$
		288 → 290	−0.417	39.8		$d_{xz}, \pi \rightarrow \pi^*$
340.1	367.1	289 → 292	0.428	39.7	0.2600	$\pi \rightarrow \sigma^*, d_{x^2-y^2}{}^*$
		289 → 291	−0.333	30.8		$\pi \rightarrow \pi^*, d_{x^2-y^2}{}^*$
331.3	357.6	287 → 292	0.337	24.8	0.0027	$d_{yz}, \pi \rightarrow \sigma^*, d_{x^2-y^2}{}^*$
		288 → 293	0.266	19.6		$d_{xz}, \pi \rightarrow \pi^*, d_{z^2}, \sigma^*(CN)$
326.3	352.2	287 → 293	0.381	28.2	0.0127	$d_{yz}, \pi \rightarrow \sigma^*, d_{x^2-y^2}{}^*$
		288 → 292	0.238	17.6		$d_{xz}, \pi \rightarrow \sigma^*, d_{x^2-y^2}{}^*$
316.0	341.0	289 → 293	0.602	59.8	0.0203	$\pi \rightarrow \pi^*, d_{z^2}{}^*, \sigma^*(CN)$
		289 → 294	0.283	28.1		$\pi \rightarrow \pi^*$
313.3	338.1	287 → 290	0.606	56.3	0.0174	$d_{yz}, \pi \rightarrow \pi^*$
		288 → 291	0.202	18.8		$d_{xz}, \pi \rightarrow \pi^*, d_{x^2-y^2}{}^*$
297.2	320.8	288 → 291	0.558	39.0	0.0277	$d_{xz}, \pi \rightarrow \pi^*, d_{x^2-y^2}{}^*$
		289 → 294	0.261	18.2		$\pi \rightarrow \pi^*$
295.5	319.0	286 → 290	0.640	72.7	0.0229	$d_{xz}, \pi(CN) \rightarrow \pi^*$
		285 → 290	−0.134	15.3		$d_{yz}, \pi(CN) \rightarrow \pi^*$
287.0	309.7	289 → 294	0.526	39.9	0.0395	$\pi \rightarrow \pi^*$
		284 → 290	−0.289	21.9		$\pi, \pi(CN) \rightarrow \pi^*$
276.3	298.2	283 → 290	0.553	39.8	0.0033	$\pi, \sigma, \pi(CN) \rightarrow \pi^*$
		284 → 290	0.187	13.4		$\pi, \pi(CN) \rightarrow \pi^*$
274.1	295.9	273 → 293	0.353	21.9	0.0077	$d_{xy}, \pi \rightarrow \pi^*, d_{z^2}, \sigma^*(CN)$
		283 → 290	−0.233	14.4		$\pi, \sigma, \pi(CN) \rightarrow \pi^*$
271.6	293.1	285 → 290	−0.396	24.3	0.0805	$d_{yz}, \pi(CN) \rightarrow \pi^*$
		281 → 290	−0.288	17.7	0.0805	$\pi(CN) \rightarrow \pi^*$
266.4	287.5	282 → 290	−0.482	36.8	0.1302	$\pi(CN) \rightarrow \pi^*$
		281 → 290	0.341	26.1		$\pi(CN) \rightarrow \pi^*$
263.5	284.4	280 → 290	0.532	45.2	0.0116	$\pi, \pi(CN) \rightarrow \pi^*$
		285 → 290	0.305	25.9		$d_{yz}, \pi(CN) \rightarrow \pi^*$
261.6	282.4	285 → 290	−0.401	29.6	0.0414	$d_{yz}, \pi(CN) \rightarrow \pi^*$
		284 → 290	0.388	28.7		$\pi, \pi(CN) \rightarrow \pi^*$
256.7	277.1	288 → 292	0.375	21.7	0.0205	$d_{xz}, \pi \rightarrow \sigma^*, d_{x^2-y^2}{}^*$
		273 → 290	0.311	18.0		$d_{xy}, \pi \rightarrow \pi^*$
255.3	275.5	289 → 295	0.563	53.2	0.0029	$\pi \rightarrow \pi^*(-CH_2CO_2Me)$
		273 → 290	−0.253	24.0		$d_{xy}, \pi \rightarrow \pi^*$

[a] Orbital assignments for transitions, e.g., $(d_{xz}, \pi) \rightarrow (\sigma^*, d_{x^2-y^2}{}^*)$, should be read as follows. Occupied orbital: d_{xz}, π (metal $3d_{xz}$ AO mixed with corrin π MO). Unoccupied orbital: $\sigma^*, d_{x^2-y^2}{}^*$ (corrin σ^* MO mixed with out-of-phase $3d_{x^2-y^2}$ AO). Molecular orbitals with no descriptor other than π or σ refer to π- and σ-symmetry MOs of the corrin ring. [b] A full list of transitions for each excited state is available in the Supporting Information. [c] Unmodified excited state energy. [d] Excited state energy scaled to match the most intense experimental transition (scale factor = 1.0794). [e] Oscillator strength (unmodified).

approach, moreover, is that the spectrum is adequately explained by singlet ground and excited states.

A total of 22 excited singlet states were located between 250 and 500 nm for DCCbs and DCSYCbs. The principal transitions responsible for each electronic state are assigned and listed in Tables 5 and 6; full lists of all electronic transitions are available in the Supporting Information (Tables S9 and S10). Calculated and experimental spectra are compared in Figure 11. The calculated

dx.doi.org/10.1021/ic200285k |*Inorg. Chem.* 2011, 50, 8700–8718

Table 6. DFT-Calculated Excited Singlet States (*in Vacuo*) and Main Transition Assignments for DCSYCbs (TD-DFT Method, PBE1PBE/6-311G Level of Theory)[a,b]**

λ^c/nm	$\lambda^{s\,d}$/nm	MOs	largest coeff	%	f^e	transition assignment
439.5	485.8	289 → 290	0.546	66.6	0.1092	$\pi \rightarrow \pi^*$
		289 → 293	0.165	20.1		$\pi \rightarrow \sigma^*$, $d_{x^2-y^2}{}^*$
418.3	462.3	289 → 290	0.317	18.5	0.0467	$\pi \rightarrow \pi^*$
		289 → 293	−0.18	10.5		$\pi \rightarrow \sigma^*$, $d_{x^2-y^2}{}^*$
405.7	448.4	287 → 293	0.234	13.2	0.0153	d_{yz}, π(CN) → σ^*, $d_{x^2-y^2}{}^*$
		287 → 294	−0.234	13.2		d_{yz}, π(CN) → σ^*, $d_{z^2}{}^*$, σ^*(CN)
401.1	443.3	288 → 292	0.201	12.7	0.0102	d_{xz}, π, π(CN) → π^*, σ^*, $d_{x^2-y^2}{}^*$
		288 → 294	0.193	12.2		d_{xz}, π, π(CN) → σ^*, $d_{z^2}{}^*$, σ^*(CN)
350.7	387.6	289 → 292	0.421	31.1	0.0070	$\pi \rightarrow \pi^*$, σ^*, $d_{x^2-y^2}{}^*$
		289 → 294	0.252	18.6		$\pi \rightarrow \sigma^*$, $d_{z^2}{}^*$, σ^*(CN)
334.5	369.7	289 → 291	0.594	69.4	0.0044	$\pi \rightarrow \sigma^*$, π^*, $d_{x^2-y^2}{}^*$
		287 → 293	−0.149	17.4		d_{yz}, π(CN) → σ^*, $d_{x^2-y^2}{}^*$
330.3	365.0	288 → 294	0.307	20.0	0.0013	d_{xz}, π, π(CN) → σ^*, $d_{z^2}{}^*$, σ^*(CN)
		288 → 293	−0.251	16.3		d_{xz}, π, π(CN) → σ^*, $d_{x^2-y^2}{}^*$
312.5	345.4	289 → 293	0.369	23.8	0.0011	$\pi \rightarrow \sigma^*$, $d_{x^2-y^2}{}^*$
		289 → 294	−0.246	15.9		$\pi \rightarrow \sigma^*$, $d_{z^2}{}^*$, σ^*(CN)
307.7	340.1	289 → 293	0.417	31.3	0.0062	$\pi \rightarrow \sigma^*$, $d_{x^2-y^2}{}^*$
		289 → 292	−0.355	26.6		$\pi \rightarrow \pi^*$, σ^*, $d_{x^2-y^2}{}^*$
297.2	328.5	289 → 294	0.405	27.2	0.0199	$\pi \rightarrow \sigma^*$, $d_{z^2}{}^*$, σ^*(CN)
		288 → 290	−0.333	22.3		d_{xz}, π, π(CN) → π^*
290.4	321.0	288 → 290	0.459	36.3	0.1895	d_{xz}, π, π(CN) → π^*
		289 → 294	0.252	19.9		$\pi \rightarrow \sigma^*$, $d_{z^2}{}^*$, σ^*(CN)
283.7	313.6	287 → 290	0.601	65.5	0.0021	d_{yz}, π(CN) → π^*
		289 → 294	−0.174	19.0		$\pi \rightarrow \sigma^*$, $d_{z^2}{}^*$, σ^*(CN)
268.3	296.5	274 → 294	0.217	12.6	0.0050	d_{xy}, π, π(−CH^{2}CO$_2$Me) → σ^*, $d_{z^2}{}^*$, σ^*(CN)
		275 → 294	−0.217	12.6		d_{xy}, π, π(−CH^{2}CO$_2$Me), π(CN) → σ^*, $d_{z^2}{}^*$, σ^*(CN)
263.7	291.5	286 → 290	0.652	82.5	0.0522	d_{xz}, π(CN) → π^*
		288 → 290	−0.139	17.5		d_{xz}, π, π(CN) → π^*
254.0	280.7	289 → 295	0.654	72.0	0.0001	$\pi \rightarrow \pi^*$(−$CH_2CH_2CO_2Me$)
		289 → 296	−0.255	28.0		$\pi \rightarrow \pi^*$(−$CH_2CH_2CO_2Me$), π^* (−CH_2CO_2Me)
253.5	280.2	283 → 290	0.448	34.6	0.0234	π, d_{yz}, π(CN) → π^*
		285 → 290	0.373	28.8		d_{xz}, π(lactone), π(CN) → π^*
252.4	279.0	281 → 290	0.578	43.3	0.0042	σ, π(CN) → π^*
		282 → 290	0.171	12.8		π, σ(CN) → π^*
251.1	277.5	288 → 291	0.588	52.6	0.0024	d_{xz}, π, π(CN) → σ^*, π^*, $d_{x^2-y^2}{}^*$
		281 → 290	0.145	12.9		σ, π_x(CN) → π^*
248.4	274.6	289 → 296	0.64	64.2	0.0002	$\pi \rightarrow \pi^*$(−$CH_2CH_2CO_2Me$), π^* (−CH_2CO_2Me)
		289 → 295	0.254	25.5		$\pi \rightarrow \pi^*$(−$CH_2CH_2CO_2Me$)
248.2	274.3	280 → 290	0.525	39.3	0.0026	σ, π_y(CN) → π^*
		285 → 290	−0.32	23.9		d_{xz}, π(lactone), π(CN) → π^*
241.02	266.40	285 → 290	0.354	17.3	0.0039	d_{xz}, π(lactone), π(CN) → π^*
		280 → 290	0.333	16.3		σ, π_y(CN) → π^*
240.99	266.37	284 → 290	−0.589	42.0	0.0008	π(−$CH_2CH_2CO_2Me$), σ(CN) → π^*
		285 → 290	−0.176	12.5		d_{xz}, π(lactone), π(CN) → π^*

[a] Orbital assignments for transitions, e.g., (d_{xz}, π, π(CN)) → (σ^*, $d_{x^2-y^2}{}^*$), should be read as follows. Occupied orbital: d_{xz}, π, π(CN) (metal $3d_{xz}$ AO mixed with corrin π MO and axial cyanide π MOs). Unoccupied orbital: σ^*, $d_{x^2-y^2}{}^*$ (corrin σ^* MO mixed with out-of-phase $3d_{x^2-y^2}$ AO). Molecular orbitals with no descriptor other than π or σ refer to π- and σ-symmetry MOs of the corrin ring. [b] A full list of transitions for each excited state is available in the Supporting Information. [c] Unmodified excited state energy. [d] Excited state energy scaled to match the most intense experimental transition (scale factor = 1.1053). [e] Oscillator strength (unmodified).

excited state energies were systematically overestimated by ≈0.27 eV relative to the experimental state energies by the current TD-DFT simulations, as were the molar absorptivities, ε. To facilitate spectral comparisons and band assignments, the calculated spectra of Figure 11 were scaled to fit the experimental γ-band energy and intensity in each case (the scale factors are given in

dx.doi.org/10.1021/ic200285k |*Inorg. Chem.* 2011, 50, 8700–8718

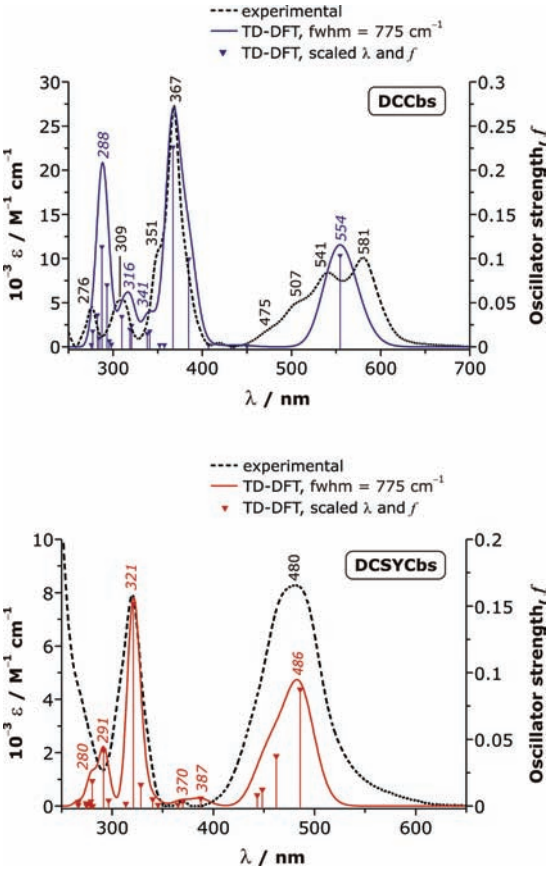

Figure 11. TD-DFT electronic spectra (22 singlet excited states calculated *in vacuo* at the PBE1PBE/6-311+G** level of theory) for DCCbs (top) and DCSYCbs (bottom). The experimental spectra (corrected for background absorption) are shown as dashed curves in both cases. To facilitate comparison, the DFT-calculated spectra have been scaled to match the experimental γ bands for both compounds (λ and ε scale factors: 1.0794 and 0.692, respectively, DCCbs; 1.1053 and 0.278, respectively, DCSYCbs). For the calculated spectra, individual singlet states are shown as vertical lines with intensities in either of the *y*-axis units; the spectral envelope represents the summation of the component bands each having a 775 cm^{-1} width at half height. Band maxima are indicated.

the figure caption). We note that the PBE1PBE/6-311G(d,p) hybrid functional and non-ECP basis set used here on complete molecular structures collectively give more accurate excited state energies than the B3LYP/6-31G(d)-VTZ(Co) simulations reported on a simplified [Co(corrin)$(CN)_2$] model system, which required that transition energies be scaled by ≈0.5 eV.[31]

For DCCbs, the shape and fundamental features of the scaled calculated spectrum match the experimental spectrum reasonably well for λ > 300 nm. The α-band in the calculated spectrum occurs ≈26 nm to the blue of the experimental band maximum at 555 nm (this despite scaling all transition energies by a factor that allows the γ-band energy to match the experimental value). From Table 5, the α-band is due to a pure $\pi \rightarrow \pi^*$ transition involving promotion of an electron from the HOMO (MO 289) to the LUMO (MO 290), Figure 10. The second excited state is calculated to lie at a scaled wavelength of 450 nm and originates from mainly 3d$\pi \rightarrow (\sigma^*, d_{x^2-y^2})$ transitions. The largest transition dipole for this excited state corresponds to a $d_{xy} \rightarrow d_{x^2-y^2}$ excitation that involves metal orbitals that are mixed with σ-symmetry MOs of the corrin. This band is obscured in the experimental spectrum of DCCbs by the third (475 nm) vibrational overtone of the α-band as a result of its weak oscillator strength, consistent with its mainly d−d character. The second excited electronic state of DCCbs equates approximately with the ligand field parameter Δ_O (≈22 222 cm^{-1}) of a simple octahedral Co(III) ion. This band was not found in the Gaussian deconvolution of the experimental spectrum (Figure 3) because of its low intensity relative to the surrounding $\pi \rightarrow \pi^*$ bands. The absence of any calculated excited singlet states between 555 and 450 nm strongly suggests that the β-band (541 nm) and lower-intensity bands at 507 and 475 nm in the experimental spectrum of DCCbs are a vibrational progression of the α-band. As noted earlier, the experimental bands at ~436 and 407 nm are normally assigned to the D and E bands of the corrin, respectively;[31] from Table 5, these are due to 3d$\pi \rightarrow \sigma^*$ and 3d$\pi \rightarrow \pi^*$ transitions, which account for their low intensity. The D band in the experimental spectrum arises from near superposition of excited states 3 and 4 of the system at 436 and 432 nm, respectively (Table 5); these are unresolved by the Gaussian deconvolution. The γ-band of DCCbs (367 nm, seventh excited state) is an admixture of $\pi \rightarrow \sigma^*$ and $\pi \rightarrow \pi^*$ transitions between the HOMO and the LUMO + 1 and LUMO + 2 levels of the corrin (the latter unoccupied MOs are antibonding combinations of ligand MOs with the $3d_{x^2-y^2}$ AO of the metal ion). Since the 3d orbitals are not heavily mixed with the HOMO, the transitions have much more significant $\pi \rightarrow \pi^*$ than d−d character and the oscillator strength is large. The two bands of lesser intensity flanking the γ-band noted above (excited states 6 and 8 at 385 and 358 nm, respectively, in Table 5) have mixed character, $\pi \rightarrow (\sigma^*, d_{x^2-y^2})$ as well as d$\pi,\pi \rightarrow \pi^*$, and, in the case of the 358-nm band, involve a transition to a MO with significant d_{z^2}* and σ^*(CN) character (MO 293 or LUMO + 3); hence, there is some charge-transfer character (involving the equatorial and axial ligands) to this state.

The rather intense shoulder at 351 nm in the experimental spectrum of DCCbs has no counterpart in the DFT-calculated spectrum; the oscillator strengths of the calculated transitions in this region of the spectrum (Figure 11) are, in fact, an order of magnitude too low to account for this band. Since the present DFT simulations do not predict transitions to vibrational levels of an excited electronic state, we conclude that the 351 nm shoulder probably corresponds to a vibrational progression of the γ-band overlapped with the low-intensity bands for excited states 8 (see above) and 9 ($\pi \rightarrow (\sigma^*, d_{x^2-y^2})$).

Finally for DCCbs, the calculated excited states from 319 to 282 nm (with highest intensity at excited state 18, 288 nm) sum into a band that matches the experimentally observed band at 276 nm neither in energy nor intensity. This closely spaced set of excited states are seen to comprise (Table 5) mainly comparatively unmixed transitions of the type π(CN) $\rightarrow \pi^*$ and may be termed ligand-to-ligand charge-transfer bands (LLCT) in which an electron located primarily in a π-symmetry axial ligand MO is transferred to the π^* MO of the equatorial ligand (corrin macrocycle in this case). In the TD-DFT simulations reported by Andruniów et al.,[122] this type of long-range charge-transfer (LRCT) band was observed for an excited state involving promotion of an electron from the axial adenosyl ligand to the corrin π^* MO of a model adenosylcobalamin derivative. These authors similarly found rather poor agreement between the energies (and oscillator strengths) of the calculated and experimental bands associated with this CT state. It appears that LRCT

dx.doi.org/10.1021/ic200285k |*Inorg. Chem.* 2011, 50, 8700–8718

bands are generally difficult to accurately predict by TD-DFT methods.[122−124] That said, the π(CN) → π^* LLCT band for DCCbs is not that poorly predicted in our simulations, perhaps because the MOs involved are not particularly far apart in space, especially if there is some loss of intensity in the experimental spectrum (Figure 11) due to an overcompensated background correction.

The scaled DFT-calculated spectrum of DCSYCbs is shown superimposed on the experimental UV−vis spectrum in Figure 11 (bottom plot). The λ and ε scale factors required to overlay the simulated and experimental γ-band envelopes are larger than those used for the spectrum of DCCbs, and there is generally poorer agreement between the theoretical and experimental oscillator strengths for this compound. However, there is fair agreement between the scaled calculated excited state energies and the experimental energies between 300 and 500 nm. The α-band of the scaled theoretical spectrum (486 nm) is close in energy to that of the experimental spectrum (≈492 nm), and the generally broad nature of the visible spectrum is reasonably well reproduced in the calculations. In distinct contrast to DCCbs, the α-band of DCSYCbs is not a pure $\pi \rightarrow \pi^*$ transition (Table 6) and is of mixed character. Two thirds of the transition dipole moment derives from a $\pi \rightarrow \pi^*$ transition and another 20% is due to a $\pi \rightarrow (\sigma^*, d_{x^2-y^2})$ transition. Excited states 2−4 are located between 462 and 443 nm and have an intensity ratio (and energy spacing) that might be mistaken for a vibrational progression of the α-band, especially since this type of spectral feature is so prominent for DCCbs. This is not the case; electronic states 2−4 are genuine singlet excited states of the chromophore with $\pi \rightarrow (\sigma^*, d_{x^2-y^2})$ or d → d* character mixed in with $\pi \rightarrow \sigma^*$ or $\pi \rightarrow \pi^*$ character. The fact that 67% of the α-band (excited state 1) consists of a strongly allowed $\pi \rightarrow \pi^*$ transition of the corrin could, however, allow for a fairly intense vibrational progression in the experimental spectrum. One problem with the TD-DFT method is that it does not calculate the vibrational states that may be associated with an excited electronic state for a chromophore. However, it should now be clear that if the above singlet excited states (at 462, 448, and 443 nm) of DCSYCbs were buried beneath a narrowly spaced vibrational progression of the α-band in the experimental spectrum, then a broad featureless band would be observed due to overlapping states of different origins. This seems to be a reasonable explanation for the key difference between the spectra of DCSYCbs and DCCbs in the visible region of the spectrum; in DCSYCbs the diminished π-delocalization of the corrin macrocycle in DCSYCbs gives rise to a first excited singlet state transition (the α-band) at a shorter wavelength than that in DCCbs and the $\pi \rightarrow \pi^*$ and d → d* transitions exhibit a strong degree of overlap. The D band of DCSYCbs evidently comprises excited states 6 and 7 at 370 and 365 nm, respectively (Table 6); these are in excellent agreement with the Gaussian component of Figure 3 at 370 nm. The transitions responsible for the D band depart from corrin π MOs that are heavily mixed with metal dπ and axial cyanide π MOs, as was the case for DCCbs. The destination MOs for these transitions are corrin σ^* and B* orbitals mixed with the $3d_{x^2-y^2}$ and $3d_{z^2}$ metal AOs as well as axial cyanide σ^* MOs for at least one of the transitions. The E band of DCSYCbs comprises excited states 8 and 9 at 345 and 340 nm, which compare favorably with the Gaussian component of the experimental absorption spectrum at 352 nm. In contrast to the D band, the transitions responsible for these excited states all depart from the HOMO, which is a relatively unmixed π orbital of the corrin macrocycle. The destination MOs have mixed isosurfaces with corrin $\sigma^*/3d_{z^2}$ and $\sigma^*/3d_{x^2-y^2}$ character such that the E band may be broadly classified as $\pi \rightarrow \sigma^*$/d* in origin.

The γ-band of DCSYCbs at 321 nm (excited state 11) involves mainly a transition from the HOMO − 1 to the LUMO (36%) and a transition from the HOMO to the LUMO + 4 level (20%). The main transition of the band has appreciable dπ,π, and π(CN) character for the occupied orbital and essentially pure corrin π^* character for the unoccupied orbital. The γ-band of DCSYCbs is thus different in origin to that of DCCbs, which had no contribution from the axial cyanide π MOs in the occupied or unoccupied MOs involved in the transition. The (dπ,π) → π^* nature of the principal transition for the γ-band of the yellow corrin derivative accounts for its diminished oscillator strength (0.1895) relative to that calculated for DCCbs (0.2600), in agreement with the intensity drop seen in the experimental spectrum (Figure 3).

The γ-band envelope of the DFT-calculated spectrum of DCSYCbs is sharper and less asymmetric than that of the experimental band. The latter band's asymmetry suggests the presence of a shoulder of moderate intensity on the short-wavelength side of the band. Gaussian deconvolution of the experimental spectrum has allowed us to resolve this obscured band, which has a maximum at 306 nm. From its intensity and lack of a DFT-calculated counterpart, this band probably arises from the first vibrational overtone of the γ-band.

Finally, the calculated spectrum of DCSYCbs has an array of lower-intensity transitions to the blue of the γ-band between 266 and 314 nm; these culminate in two maxima for the simulated spectral envelope at 291 and 280 nm, with the latter being visible as a shoulder in Figure 11. The calculated spectral envelope differs significantly in shape from that of DCCbs in this region; for example, the strong sharp band at 288 nm in the calculated spectrum of DCCbs is reduced to a shoulder in the case of DCSYCbs. Inspection of the transition assignments in Tables 4 and 5 reveals that the orbital parentages of the transitions are quite different. LLCT transitions for DCSYCbs are still present, but in contrast to DCCbs, they tend to involve heavily mixed occupied orbitals. The array of calculated transitions is thus more complex to analyze for DCSYCbs. However, three noteworthy features merit discussion. First, pure π(CN) → π^* LLCT transitions, as calculated for DCCbs, are absent. Instead, the transitions producing excited states 14 (292 nm) and 17 (279 nm) depart from occupied MOs that involve axial cyanide π MOs mixed with either dπ AOs or corrin π/σ MOs. The oscillator strengths are consequently lower relative to a pure π(CN) → π^* LLCT transition. Second, for many excited states at wavelengths <300 nm, the transitions involve π^* MOs of the corrin mixed with one or more π^* components of the ester side-chains. For example, excited state 15 (281 nm) is due to a $\pi \rightarrow \pi^*$ ($-CH_2CH_2CO_2Me$) transition; this involves a longer-range electron transfer from a corrin π MO (the HOMO) to the π antibonding MO of the ester carbonyl of an appended side chain group. The oscillator strengths are not high. The calculated spectrum of DCCbs had only one such excited state (276 nm, Table 5) in contrast to the four calculated for DCSYCbs. This presumably reflects the disruption of the π-delocalization of the corrin as well as the change in overall shape and symmetry of the chromophore due to the presence of the lactone ring. Third, the lactone ring of DCSYCbs becomes directly involved in several excited states for the yellow corrin derivative. The first of these is at 280 nm (excited state 16) where 29% of the excited state

derives from a d_{xz}, π(lactone), π(CN) $\rightarrow \pi^*$ transition. Other excited states with this transition as a major component include those at 274.3, 266.40, and 266.37 nm. The lactone ring π-symmetry MO component is mixed with the d_{xz} AO and π MOs of the axial cyanide ions in the occupied MO from which the transition departs (i.e., the HOMO − 4 level). Finally, the highest energy excited state for DCSYCbs (266.37 nm) has a rather unusual principal transition (42%) which involves an occupied MO with a π-symmetry component on an ester side chain mixed with a σ-symmetry component on the axial cyanide ligands.

CONCLUSIONS

Cis effects are important in corrin chemistry. We have previously shown (see Introduction) the following: The substitution of C10 H in cobalamins by Cl causes the pK_a of coordinated H_2O to drop and affects the kinetics and thermodynamics of the binding of exogenous ligands to the metal ion.[26] The C10−Cl bond length in X-10-ClCbls depends strongly on the polarizability of the axial ligand, X.[19] Substitution of the C10 H by an electron-withdrawing group deactivates the axial coordination site toward ligand substitution.[33] We have extended our investigation into these *cis* effects and prepared and characterized DCSYCbs, (5*R*,6*R*)-Coα,Coβ-dicyano-5,6-dihydro-5-hydroxy-heptamethylcob(III)yrinate-*c*,6-lactone, from DCCbs. X-ray data confirm disruption of the conjugated π-system of the normal corrin macrocycle through the formation of a hydroxyl group at C5 and a lactone at C6 by the *c* side chain of the corrin. The ^{13}C NMR spectra for DCSYCbs have been assigned using 2D NMR methods. DFT-calculated shielding tensors (GIAO method) were used to definitively assign the inequivalent chemical shifts of the axial cyanide carbons in both cobester derivatives. The ^{59}Co chemical shifts and signal linewidths of DCCbs and DCSYCbs differ significantly; the ^{59}Co nucleus of DCCbs is more shielded (by 224 ppm) than that of DCSYCbs, and the line width is narrower for the parent cobester (DCCbs). While the DFT-calculated ^{59}Co isotropic shielding constants were inaccurate, NBO population analysis revealed that the upfield chemical shift for DCCbs originates, in part, from its higher 4s orbital electron density relative to DCSYCbs. As the strength of the interaction between Co(III) and an equatorial macrocycle increases, ν_{CN} of axially coordinated CN^- shifts to lower frequency; in DCSYCbs and DCCbs ν_{CN} occurs at 2138 and 2123 cm^{-1}, respectively, and the corrin ligand in DCCbs interacts more strongly with the metal than the stable yellow corrin ligand, with its diminished conjugation. The UV−vis spectral data, the DFT-calculated MOs, and NBO population of the [CoN_4] cores are consistent with greater overlap between the corrin and the metal orbitals in DCCbs than in DCSYCbs, which gives the metal in the former a softer, more covalent character. TD-DFT methods were particularly helpful in assigning the principal and lower-intensity bands in the electronic spectra of DCCbs and DCSYCbs. The calculations allowed delineation of the experimentally observed vibrational progressions on the α- and γ-bands for both complexes by providing a picture of the spectral envelopes due to the pure vibrationless singlet excited state transitions giving rise to these bands.

ASSOCIATED CONTENT

Supporting Information. CIF data. Additional figures and tables. This material is available free of charge via the Internet at http://pubs.acs.org.

AUTHOR INFORMATION

Corresponding Authors

*E-mail: helder.marques@wits.ac.za. (H.M.M.); susan.chemaly@wits.ac. (S.M.C.); zamunroo@ukzn.ac.za. (O.Q.M.)

ACKNOWLEDGMENT

The financial assistance of the Department of Science and Technology, and the National Research Foundation, Pretoria, through the South African Research Chairs Initiative, and the University of the Witwatersrand, Johannesburg, is gratefully acknowledged (H.M.M., S.M.C.). The support of the University of KwaZulu-Natal (O.Q.M.) is gratefully acknowledged. Mrs. Marelize Ferreira and Dr. Andrew Dinsmore are thanked for recording the mass spectra.

REFERENCES

(1) Rutenberg, A. C.; Taube, H. *J. Chem. Phys.* **1952**, *20*, 825–826.
(2) Hunt, J.; Plane, R. A. *J. Am. Chem. Soc.* **1954**, *76*, 5960–5962.
(3) Swift, T. J.; Connick, R. E. *J. Chem. Phys.* **1962**, *37*, 307–320.
(4) Fiat, D.; Connick, R. E. *J. Am. Chem. Soc.* **1968**, *90*, 608–615.
(5) Dodgen, H. W.; Liu, G.; Hunt, J. P. *Inorg. Chem.* **1981**, *20*, 1002–1005.
(6) Grant, M.; Jordan, R. B. *Inorg. Chem.* **1981**, *20*, 55–60.
(7) Randall, W. C.; Alberty, R. A. *Biochemistry* **1967**, *6*, 1520–1525.
(8) Reenstra, W. W.; Jencks, W. P. *J. Am. Chem. Soc.* **1979**, *101*, 5780–5791.
(9) Balt, S.; van Herk, A. M. *Transition Met. Chem.* **1983**, *8*, 152–154.
(10) Baldwin, D. A.; Betterton, E. A.; Pratt, J. M. *J. Chem. Soc., Dalton Trans.* **1983**, 2217–2222.
(11) Marques, H. M.; Brown, K. L.; Jacobsen, D. W. *J. Biol. Chem.* **1988**, *263*, 12378–12383.
(12) Marques, H. M.; Egan, T. J.; Marsh, J. H.; Mellor, J. R.; Munro, O. Q. *Inorg. Chim. Acta* **1989**, *166*, 249–255.
(13) Stochel, G.; van Eldik, R.; Kunkely, H.; Vogler, A. *Inorg. Chem.* **1989**, *28*, 4314–4318.
(14) Stochel, G.; van Eldik, R. *Inorg. Chem.* **1990**, *29*, 2075–2077.
(15) Marques, H. M. *J. Chem. Soc., Dalton Trans.* **1991**, 1437–1442.
(16) Marques, H. M.; Bradley, J. C.; Campbell, L. A. *J. Chem. Soc., Dalton Trans.* **1992**, 2019–2027.
(17) Waddington, M. D.; Finke, R. G. *J. Am. Chem. Soc.* **1993**, *115*, 4629–4640.
(18) Marques, H. M.; Knapton, L. *J. Chem. Soc., Dalton Trans.* **1997**, 3827–3833.
(19) Brown, K. L.; Cheng, S.; Zou, X.; Zubkowski, J. D.; Valente, E. J.; Knapton, L.; Marques, H. M. *Inorg. Chem.* **1997**, *36*, 3666–3675.
(20) Hamza, M. S. A.; Zou, X.; Brown, K. L.; van Eldik, R. *Inorg. Chem.* **2001**, *40*, 5440–5447.
(21) Hamza, M. S. A.; Elawady, M. A.; Marques, H. M. *S. Afr. J. Chem.* **2008**, *61*, 68–73.
(22) Jackson, W. G.; Jurisson, S. S.; McGregor, B. C. *Inorg. Chem.* **1985**, *24*, 1788–1790.
(23) Betterton, E. A. Ph.D. Thesis, University of the Witwatersrand, Johannesburg, 1982.
(24) Hamza, M. S. A.; Dücker-Benfer, C.; van Eldik, R. *Inorg. Chem.* **2000**, *39*, 3777–3783.
(25) Poon, C. K. *Coord. Chem. Rev.* **1973**, *10*, 1–35.
(26) Knapton, L.; Marques, H. M. *Dalton Trans.* **2005**, 889–895.
(27) Perry, C. B.; Fernandes, M. A.; Brown, K. L.; Zou, X.; Valente, E. J.; Marques, H. M. *Eur. J. Inorg. Chem.* **2003**, 2095–2107.
(28) Day, P. *Coord. Chem. Rev.* **1967**, *2*, 99–108.
(29) Giannotti, C. In *B12*; Dolphin, D., Ed.; Wiley: New York, 1982; pp 393−430.
(30) Pratt, J. M. In *Chemistry and Biochemistry of B12*; Banerjee, R., Ed.; John Wiley & Sons: New York, 1999; pp 113−164.

(31) Andruniow, T.; Kozlowski, P. M.; Zgierski, M. Z. *J. Chem. Phys.* **2001**, *115*, 7522–7533.
(32) Perry, C. B.; Marques, H. M. *S. Afr. J. Chem.* **2005**, *58*, 9–15.
(33) Marques, H. M.; Knapton, L.; Zou, X.; Brown, K. L. *J. Chem. Soc., Dalton Trans.* **2002**, 3195–3200.
(34) Gossauer, A.; Grüning, B.; Ernst, L.; Becker, W.; Sheldrick, W. S. *Angew. Chem., Int. Ed. Engl.* **1977**, *16*, 481–482.
(35) Grüning, B.; Holze, G.; Jenny, T.; Nesvadba, P.; Gossauer, A.; Ernst, L.; Sheldrick, W. S. *Helv. Chim. Acta* **1985**, *68*, 1754–1770.
(36) Chemaly, S. M.; Florczak, M.; Dirr, H.; Marques, H. M. *Inorg. Chem.* **2011**in press.
(37) *APEX2, v. 2.0-1*; Bruker AXS Inc.: Madison, WI, 2005.
(38) *SAINT+ (includes XPREP and SADABS), v. 6.02*; Brüker AXS Inc.: Madison, WI, 1999.
(39) Sheldrick, G. M. *SADABS*; University of Göttingen: Germany, 1996.
(40) Werthemann, L. PhD, ETH, Zürich, 1968.
(41) Byers, J. A. http://www.chemical-ecology.net/java/solvents.htm (accessed January 20, 2009).
(42) Tahara, K.; Shimakoshi, H.; Tanaka, A.; Hisaeda, Y. *J. Chem. Soc., Dalton Trans.* **2010**, *39*, 3035–3042.
(43) Markwell, A. J.; Pratt, J. M.; Shaikjee, S. S.; Toerien, J. G. *J. Chem. Soc., Dalton Trans.* **1987**, 1349–1357.
(44) Hamza, M. S. A. *J. Inorg. Biochem.* **1998**, *69*, 269–274.
(45) *SHELXTL (includes XS, XL, XP, XSHELL), v. 5.1*; Brüker AXS Inc.: Madison, WI, 1999.
(46) *MERCURY, 1.4.2*; CCDC: Cambridge, U.K., 2001.
(47) Farrugia, L. J. *J. Appl. Crystallogr.* **1997**, *30*, 565.
(48) Frisch, M. J.; Trucks, G. W.; Schlegel, H. B.; Scuseria, G. E.; Robb, M. A.; Cheeseman, J. R.; Montgomery, J. J. A.; Vreven, T.; Kudin, K. N.; Burant, J. C.; Millam, J. M.; Iyengar, S. S.; Tomasi, J.; Barone, V.; Mennucci, B.; Cossi, M.; Scalmani, G.; Rega, N.; Petersson, G. A.; Nakatsuji, H.; Hada, M.; Ehara, M.; Toyota, K.; Fukuda, R.; Hasegawa, J.; Ishida, M.; Nakajima, T.; Honda, Y.; Kitao, O.; Nakai, H.; Klene, M.; Li, X.; Knox, J. E.; Hratchian, H. P.; Cross, J. B.; Adamo, C.; Jaramillo, J.; Gomperts, R.; Stratmann, R. E.; Yazyev, O.; Austin, A. J.; Cammi, R.; Pomelli, C.; Ochterski, J. W.; Ayala, P. Y.; Morokuma, K.; Voth, G. A.; Salvador, P.; Dannenberg, J. J.; Zakrzewski, V. G.; Dapprich, S.; Daniels, A. D.; Strain, M. C.; Farkas, O.; Malick, D. K.; Rabuck, A. D.; Raghavachari, K.; Foresman, J. B.; Ortiz, J. V.; Cui, Q.; Baboul, A. G.; Clifford, S.; Cioslowski, J.; Stefanov, B. B.; Liu, G.; Liashenko, A.; Piskorz, P.; Komaromi, I.; Martin, R. L.; Fox, D. J.; Keith, T.; Al-Laham, M. A.; Peng, C. Y.; Nanayakkara, A.; Challacombe, M.; Gill, P. M. W.; Johnson, B.; Chen, W.; Wong, M. W.; Gonzalez, C.; Pople, J. A. *Gaussian 03, 2003*; Gaussian Inc.: Pittsburgh, PA, 2004.
(49) Perdew, J. P.; Burke, K.; Ernzerhof, M. *Phys. Rev. Lett.* **1996**, *77*, 3865–3868.
(50) Ruud, K.; Helgaker, T.; Bak, K. L.; Jørgensen, P.; Jensen, H. J. A. *J. Chem. Phys.* **1993**, *99*, 3847–3859.
(51) Cossi, M.; Scalmani, G.; Rega, N.; Barone, V. *J. Chem. Phys.* **2002**, *117*, 43–54.
(52) Stratmann, R. E.; Scuseria, G. E.; Frisch, M. J. *J. Chem. Phys.* **1998**, *109*, 8218–8224.
(53) *Igor Pro, 6.11*; WaveMetrics, Inc.: Portland, OR, 2007.
(54) George, P.; Irvine, D. H.; Glauser, S. C. *Ann. N. Y. Acad. Sci.* **1960**, *88*, 393–415.
(55) Offenhartz, B. H.; George, P. *Biochemistry* **1963**, *2*, 142–145.
(56) Hayward, G. C.; Hill, H. A. O.; Pratt, J. M.; Vanston, N. J.; Williams, R. J. P. *J. Chem. Soc. A* **1965**, 6485–6493.
(57) Kräutler, B.; Caderas, C.; Konrat, R.; Puchberger, M.; Kratky, C. *Helv. Chim. Acta* **1995**, *78*, 581–599.
(58) Shimakoshi, H.; Abiru, M.; Izumi, S.; Hisaeda, Y. *Chem. Commun.* **2009**, 6427–6429.
(59) Hamza, M. S. A. *Personal communication*.
(60) Bonnett, R.; Godfrey, J. M.; Math, V. B.; Edmond, E.; Evans, H.; Hodder, O. J. R. *Nature* **1971**, *229*, 473–476.
(61) Bonnett, R.; Godfrey, J. M.; Math, V. B. *J. Chem. Soc. C* **1971**, 3736–3743.
(62) Stoeckli-Evans, H.; Edmond, E.; Hodgkin, D. C. *J. Chem. Soc., Perkin Trans. 2* **1972**, 605–614.
(63) Brown, K. L.; Evans, D. R.; Zubkowski, J. D.; Valente, E. J. *Inorg. Chem.* **1996**, *35*, 415–423.
(64) Bonnett, R.; Godfrey, J. M.; Math, V. B. *J. Chem. Soc., Perkin Trans. I* **1973**, 252–257.
(65) Schiebel, H. M.; Schulten, H.-R. *Mass Spectrom. Rev* **1986**, *5*, 249–311.
(66) Gruber, K.; Jogl, G.; Klintschar, G.; Kratky, C. In *Vitamin B12 and B12-Proteins*; Krautler, B., Arigoni, D., Golding, B. J., Eds.; Wiley-VCH: Weinheim, 1998; pp 335−347.
(67) Randaccio, L.; Geremia, S.; Nardin, G.; Šlouf, M.; Srnova, I. *Inorg. Chem.* **1999**, *38*, 4087–4092.
(68) *Cambridge Structural Database (CSD), Version 5.30*; November 2008; Allen, F. H. *Acta Crystallogr.* **2002**, *B58*, 380−388.
(69) Brown, K. L. In *Chemistry and Biochemistry of B12*; Banerjee, R., Ed.; John Wiley & Sons, Inc.: New York, 1999; pp 197−237.
(70) Medek, A.; Frydman, V.; Frydman, L. *Proc. Natl. Acad. Sci. U.S.A.* **1997**, *94*, 14237–14242.
(71) Kamiya, K.; Kennard, O. *J. Chem. Soc., Perkin Trans. 1* **1982**, 2279–2288.
(72) Fischli, A.; Daly, J. J. *Helv. Chim. Acta* **1980**, *63*, 1628–1643.
(73) Dresow, B.; Schlingmann, G.; Sheldrick, G. M.; Koppenhagen, V. B. *Angew. Chem., Int. Ed. Engl.* **1980**, *19*, 321.
(74) Battersby, A. R.; Grgurina, I.; Raithby, P. R.; Egert, E.; Harms, K.; Sheldrick, G. M. *Acta Crystallogr., Sect. C* **1989**, *C45*, 1589–1593.
(75) Schlingmann, G.; Dresow, B.; Koppenhagen, V. B.; Becker, W.; Sheldrick, W. S. *Angew. Chem., Int. Ed. Engl.* **1980**, *19*, 321–322.
(76) Glusker, J. P. In *B12*; Dolphin, D., Ed.; Wiley-Interscience: New York, 1982; Vol. 1, pp 23−107.
(77) Benn, R.; Mynott, R. *Angew. Chem., Int. Ed. Engl.* **1985**, *24*, 333–335.
(78) Enrst, L. *Liebigs Ann. Chem.* **1981**, 376–387.
(79) Ernst, L.; Maag, H. *Liebigs. Ann.* **1996**, 323–326.
(80) Ernst, L. *J. Chem. Soc., Perkin Trans. 1* **1984**, 2267–2270.
(81) Gossauer, A.; Heise, K.-P.; Gotze, H.; Inhoffen, H. H. *Liebigs Ann. Chem.* **1977**, 1480–1499.
(82) Brown, K. L.; Hakimi, J. M. *Inorg. Chem.* **1984**, *23*, 1756–1764.
(83) Brown, K. L.; Brooks, H. B.; Gupta, B. D.; Victor, M.; Marques, H. M.; Scooby, D. C.; Goux, W. J.; Timkovich, R. *Inorg. Chem.* **1991**, *30*, 3430–3438.
(84) Schlingmann, G.; Dresow, B.; Ernst, L.; Koppenhagen, V. B. *Liebigs Ann. Chem.* **1981**, 2061–2066.
(85) Tavagnacco, C.; Balducci, G.; Costa, G.; Taschler, K.; von Philipsborn, W. *Helv. Chim. Acta* **1990**, *73*, 1469–1480.
(86) Nakagawa, I.; Shimanouchi, T. *Spectrochim. Acta* **1962**, *18*, 101–113.
(87) Dunbar, K. R.; Heintz, R. A. *J. Am. Chem. Soc.* **1988**, *110*, 8247–8249.
(88) Dunbar, K. R.; Heintz, R. A. In *Progress in Inorganic Chemistry*; Karlin, K. D., Ed.; John Wiley & Co: New York, 1997; Vol. 45, pp 283−391.
(89) Tsubaki, M.; Yoshikawa, S. *Biochemistry* **1993**, *32*, 164–173.
(90) Boffi, A.; Chiancone, E.; Takahashi, S.; Rousseau, D. L. *Biochemistry* **1997**, *36*, 4505–4509.
(91) Pratt, J. M. *The Inorganic Chemistry of Vitamin B12*; Academic Press: London, 1972.
(92) Brown, K. L.; Gupta, B. D. *Inorg. Chem.* **1990**, *29*, 3854–3860.
(93) Brown, K. L.; Satyanarayana, S. *Inorg. Chem.* **1992**, *31*, 1366–1369.
(94) Firth, R. A.; Hill, H. A. O.; Pratt, J. M.; Thorp, R. G.; Williams, R. J. P. *J. Chem. Soc. A* **1968**, 2428–2433.
(95) Fahmy, N.; Leverenz, A.; Hanack, M. *Synth. Met.* **1991**, *41*−*43*, 2615–2619.
(96) Dodd, D.; Johnson, M. D. *J. Chem. Soc., Dalton Trans.* **1973**, 1218–1226.
(97) Watzky, M. A.; Endicott, J. F.; Song, X.; Lei, Y.; Macatangay, A. *Inorg. Chem.* **1996**, *35*, 3463–3473.
(98) Stich, T. A.; Brooks, A. J.; Buan, N. R.; Brunold, T. C. *J. Am. Chem. Soc.* **2003**, *125*, 5897–5914.

(99) Eschenmoser, A.; Scheffold, R.; Bertele, E.; Pesaro, M.; Gschwend, H. *Proc. Roy. Soc. A* **1965**, *288*, 306–333.
(100) Runge, E.; Gross, E. K. U. *Phys. Rev. Lett.* **1984**, *52*, 997–1000.
(101) Jensen, K. P.; Ryde, U. *J. Phys. Chem. A* **2003**, *107*, 7539–7545.
(102) Kuta, J.; Patchkovskii, S.; Zgierski, M. Z.; Kozlowski, P. M. *J. Comput. Chem.* **2006**, *27*, 1429–1437.
(103) Kuta, J.; Wuerges, J.; Randaccio, L.; Kozlowski, P. M. *J. Phys. Chem. A* **2009**, *113*, 11604–11612.
(104) Kornobis, K.; Kumar, N.; Wong, B. M.; Lodowski, P.; Jaworska, M.; Andruniów, T.; Ruud, K.; Kozlowski, P. M. *J. Phys. Chem. A* **2011**, *115*, 1280–1292.
(105) Solheim, H.; Kornobis, K.; Ruud, K.; Kozlowski, P. M. *J. Phys. Chem. B* **2011**, *115*, 737–748.
(106) Gao, H.; Wei, X.; Liu, X.; Yan, T. *J. Phys. Chem. B* **2010**, *114*, 4056–4062.
(107) Gryff-Keller, A.; Dybiec, K. *Magn. Reson. Chem.* **2009**, *47*, 63–66.
(108) Niskanen, M.; Hirva, P.; Haukka, M. *J. Chem. Theory Comput.* **2009**, *5*, 1084–1090.
(109) Gancheff, J. S.; Denis, P. A.; Hahn, F. E. *Spectrochim. Acta, Part A* **2010**, *76*, 348–355.
(110) Gancheff, J. S.; Albuquerque, R. Q.; Martinez-Guerrero, A.; Pape, T.; De Cola, L.; Hahn, F. E. *Eur. J. Inorg. Chem.* **2009**, 4043–4051.
(111) Gancheff, J. S.; Denis, P. A. *J. Phys. Chem. A* **2011**, *115*, 211–218.
(112) Bühl, M. *Chem. Phys. Lett.* **1997**, *267*, 251–257.
(113) Munro, O. Q.; Camp, G. L.; Carlton, L. *Eur. J. Inorg. Chem.* **2009**, 2512–2523.
(114) Chan, J. C. C.; Au-Yeung, S. C. F. *THEOCHEM* **1997**, *393*, 93–96.
(115) Bühl, M.; Håkansson, M.; Mahmoudkhani, A. H.; Öhrstrom, L. *Organometallics* **2000**, *19*, 5589–5596.
(116) Becke, A. D. *J. Chem. Phys.* **1993**, *98*, 5648–5652.
(117) Lee, C.; Yang, W.; Parr, R. G. *Phys. Rev. B* **1988**, *37*, 785–789.
(118) Godbout, N.; Oldfield, E. *J. Am. Chem. Soc.* **1997**, *119*, 8065–8069.
(119) Veillard, A.; Pullman, B. *J. Theor. Biol.* **1965**, *8*, 307–316.
(120) Ingraham, L. L.; Fox, J. P. *Ann. N. Y. Acad. Sci.* **1969**, *153*, 738–743.
(121) Schrauzer, G. N.; Lee, L. P.; Sibert, J. W. *J. Am. Chem. Soc.* **1970**, *92*, 2997–3005.
(122) Andruniów, T.; Jaworska, M.; Lodowski, P.; Zgierski, M. Z.; Dreos, R.; Randaccio, L.; Kozlowski, P. M. *J. Chem. Phys.* **2009**, *131*, 105105.
(123) Dreuw, A.; Head-Gordon, M. *J. Am. Chem. Soc.* **2004**, *126*, 4007–4016.
(124) Tozer, D. J. *J. Chem. Phys.* **2003**, *119*, 12697–12699.